MDPI

Article

Coevolutionary Diagenesis in Tight Sandstone and Shale Reservoirs within Lacustrine-Delta Systems: A Case Study from the Lianggaoshan Formation in the Eastern Sichuan Basin, Southwest China

Nan Jiang [1,2], Xingzhi Wang [1], Huanhuan Zhou [2,3], Long Luo [2,3,*], Xianfeng Tan [2,3,*], Yixin Zhu [4], Jon Gluyas [5], Jianping Liu [2,3], Xuanbo Gao [2,3], Zhouling Li [6], Jia Wang [2,3], Xin Yu [2,3], Shanzhen Tan [2,3] and Yiting Gu [2,3]

[1] School of Geoscience and Technology, Southwest Petroleum University, Chengdu 610500, China; 2016909@cqust.edu.cn (N.J.); 198431010017@swpu.edu.cn (X.W.)

[2] College of Oil and Gas Engineering, Chongqing University of Science and Technology, Chongqing 401331, China; 2021201204@cqust.edu.cn (H.Z.); 2022022@cqust.edu.cn (J.L.); 2017022@cqust.edu.cn (X.G.); wangjia@cqust.edu.cn (J.W.); 2022201086@cqust.edu.cn (X.Y.); 2023201010@cqust.edu.cn (S.T.); 2023201018@cqust.edu.cn (Y.G.)

[3] Chongqing Key Laboratory of Complex Oil and Gas Exploration and Development, Chongqing University of Science and Technology, Chongqing 401331, China

[4] Chongqing Gas Mine, PetroChina Southwest Oil & Gas Field Company, Chongqing 401120, China; zhuyixin@petrochina.com.cn

[5] Department of Earth Sciences, Durham University, Durham DH1 3LE, UK; j.g.gluyas@durham.ac.uk

[6] Chuangqing Drilling Engineering Company Limited, CNPC, Chengdu 610066, China; lizl_dyy@cnpc.com.cn

* Correspondence: longluo@cqust.edu.cn (L.L.); 2008050@cqust.edu.cn (X.T.)

Abstract: Tight sandstone and shale oil and gas are the key targets of unconventional oil and gas exploration in the lake-delta sedimentary systems of China. Understanding the coevolutionary diagenesis of sandstone and shale reservoirs is crucial for the prediction of reservoir quality, ahead of drilling, in such systems. Thin-section description, scanning electron microscopy (SEM), X-ray diffraction (XRD), fluid inclusion analysis, porosity and permeability tests, high-pressure mercury intrusion (HPMI) measurements and nuclear magnetic resonance tests (NMR) were used to reveal the coevolutionary diagenetic mechanisms of a sandstone and shale reservoir in the Lianggaoshan Formation of the Eastern Sichuan Basin, China. The thermally mature, organic-matter-rich, dark shale of layer3 is the most important source rock within the Lianggaoshan Formation. It started to generate abundant organic acids at the early stage of mesodiagenesis and produced abundant hydrocarbons in the early Cretaceous. Porewater with high concentrations of Ca^{2+} and CO_3^{2-} entered the sandstone reservoir from dark shale as the shale was compacted during burial. Potassium feldspar dissolution at the boundary of the sandstone was more pervasive than at the center of the sandstone. The K^+ released by potassium feldspar dissolution migrated from the sandstone into mudstone. Grain-rimming chlorite coats occurred mainly in the center of the sandstone. Some silica exported from the shale was imported by the sandstone boundary and precipitated close to the shale/sandstone boundary. Some intergranular dissolution pores and intercrystal pores were formed in the shale due to dissolution during the early stages of mesodiagenesis. Chlorite coats, which precipitated during eodiagenesis, were beneficial to the protection of primary pore space in the sandstone. Calcite cement, which preferentially precipitated at the boundary of sandstone, was not conducive to reservoir development. Dissolution mainly occurred at the early stage of mesodiagenesis due to organic acids derived from the dark shale. Calcite cement could also protect some primary pores from compaction and release pore space following dissolution. The porosity of sandstone and shale was mainly controlled by the thickness of sandstone and dark shale.

Keywords: tight sandstone; lacustrine shale; coevolutionary diagenesis; lacustrine-delta system; Lianggaoshan Formation; Eastern Sichuan Basin

1. Introduction

Lacustrine tight oil and gas resources are the key targets of unconventional oil and gas exploration [1–3]. Lacustrine tight oil and gas resources are generally developed in lake-delta sedimentary systems [4,5]. These systems are characterized by interbedded thin sandstones and shales providing an assemblage of source–reservoir-cap rocks [6–8]. However, sandstone is typically of low reservoir quality, often referred to as tight [1–3]. Therefore, finding the best-quality sandstone reservoirs in such tight systems is key to the exploration of such lacustrine systems [9]. There was an obvious coupling diagenetic relationship between sandstone and shale under the combination of sandstone/shale interbeds [10–14], so the synergistic diagenetic evolution of sandstone/shale generally determined the pore space type and distribution of sandstone and shale reservoirs [10–14], and yet, tight sandstone and shale reservoirs are generally independently researched in the tight oil and gas exploration of lake-delta sedimentary systems [15–19]. The synergistic diagenetic evolution and coupling genetic mechanism of sandstone and shale reservoirs are rarely researched, which restricts the efficient exploration and development of tight oil and gas in lake-delta sedimentary systems [11–14].

In recent years, some important breakthroughs have been made in the exploration and development of Jurassic tight oil and gas in the Sichuan Basin [20,21]. The Lianggaoshan Formation, which was developed in a lake-delta sedimentary system, is a typical development target in tight sandstone gas and shale oil and characterized by source–reservoir integration, adjacent source–reservoirs, and frequent inter-layers [8,9,22]. The aim of this study was to reveal the coevolutionary mechanism of a tight sandstone and shale reservoir within the lacustrine-delta system of the Lianggaoshan Formation of the Eastern Sichuan Basin (Figure 1c) and provide evidence for reservoir quality prediction in unexplored regions.

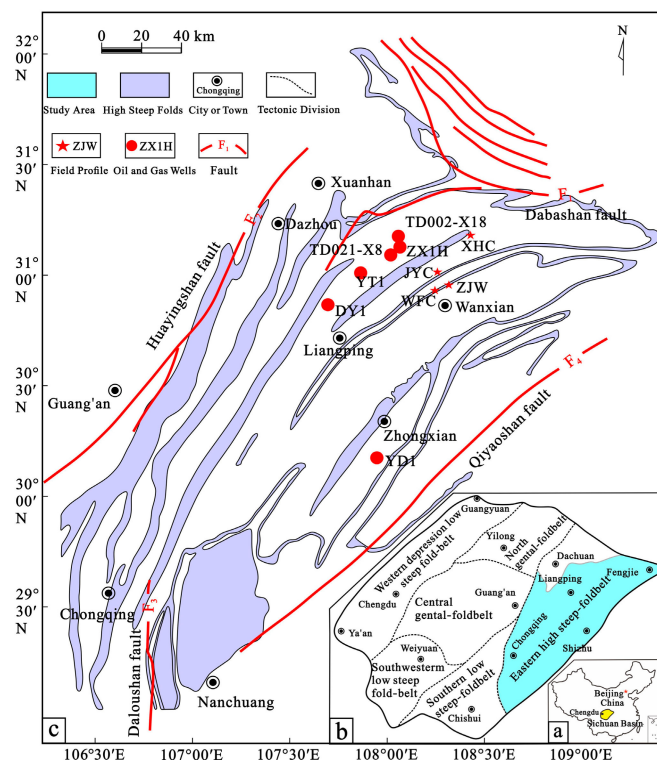**Figure 1.** Location of study area. (**a**) showing the location of Sichuan Basin in the map of China. (**b**) showing the location of high-steep fold belt in the Sichuan Basin. (**c**) showing the well location and structural characteristics of study area.

2. Geological Background

2.1. Structural Setting

The Sichuan Basin, in southwestern China, is one of the nation's important oil and gas basins (Figure 1a). The Eastern Sichuan Basin is situated in the high-steep fold belt, that extends from the Huayingshan fault to the Qiyueshan fault (Figure 1b). The intense structural folding of the eastern Sichuan Basin was mainly formed during the Himalayan period due to multiple phases of tectonic activities [18,23]. The Eastern high-steep fold belt mainly consists of many northeastern parallel narrow-steep anticlines and wide-gentle synclines (Figure 1c). Many faults and fractures mainly developed along the NE fold (main anticline), and the faults generally developed during the late Yanshanian and Himalayan cycles. These faults mainly passed through Lianggaoshan Formation, Da'anzhai Member, and Dongyuemiao Member [24–26]. These faults are the main channels for fluid migration, such as of oil and gas [27].

2.2. Stratigraphy and Sequence

The Lower Jurassic Lianggaoshan Formation thickness generally varies from 100 m to 280 m. It mainly consists of interbedded gray fine-grained sandstone and dark gray shale in the study area [22,28] (Figure 2). The Lianggaoshan Formation can be further divided into one third-order sequence, including a lowstand systems tract, a lake transgression systems tract, and a highstand systems tract [29–31] (Figure 2). The formation is divided into three members (Figure 2). The first member (Liang1) of Lianggaoshan Formation mainly consists of lowstand systems tract and lake transgression system tract [22,28]. The highstand systems tract is divided into second member (Liang2) and third member (Liang3) from the bottom to the top [22,28] (Figure 2). The lowstand systems tract can be subdivided into the first (layer1) and second layer (layer2) [22,28] (Figure 2). The lake transgression system tract, which generally comprises dark gray shale rich in organic matter, was equal to the third layer (layer3) and the most important source rock [22,28] (Figure 2). The second (Liang2) and third member (Liang3) was subdivided into fourth (layer4), fifth (layer5), sixth (layer6), seventh (layer7), eighth (layer8) and ninth (layer9) layers from the bottom to the top [22,28] (Figure 2).

2.3. Sedimentary Setting

The Lianggaoshan Formation was mainly deposited in the lake-delta sedimentary system (Figure 2). The Daba Mountain was the main provenance of Lianggaoshan Formation in the northeastern basin (Figure 1c). The layer1 and layer2 of Lianggaoshan Formation were mainly deposited in the delta front environment (Figure 2). The layer3 was mainly developed in the semi-deep and shore-shallow lacustrine facies (Figure 2). The second member (Liang2) and third member (Liang3) of Lianggaoshan Formation were deposited in the delta front facies including subaqueous distributary channel, underwater natural levee, mouth bar, distant sand bar and sheet sand [22,28] (Figure 2). The sediment of Lianggaoshan Formation was supplied by the meandering river in the study area [22,28]. The meandering river delta of Lianggaoshan Formation was characterized by the interbedded sandstone and shale with low sand–shale ratio [22,28] (Figure 2).

2.4. Oil and Gas Shows

Oil and gas shows were recorded during drilling and logging of 30 wells in this area (Figure 2). Oil and gas shows mainly consist of gas logging abnormity (number 61), leakage (number 8), gas influx (number 3), and kick (number 1) in the Lianggaoshan Formation. The oil and gas shows mainly occur in the layer3 and layer4 (Figure 2). There are 12 shows of gas logging abnormity, two leakage, one kick and one gas influx in the layer4 (Figure 2). There are 11 shows of gas logging abnormity and one gas influx in the layer5 (Figure 2). There are seven shows of gas logging abnormity and one gas influx in the layer8. There are only five shows of gas logging abnormity in the layer6 (Figure 2). Four gas logging abnormities and one leakage occurred in the layer7 (Figure 2). Four gas logging abnormities

and two gas influxes happened in the layer9 (Figure 2). Additionally, there were only three and four oil and gas shows in the layer1 and layer2 (Figure 2).
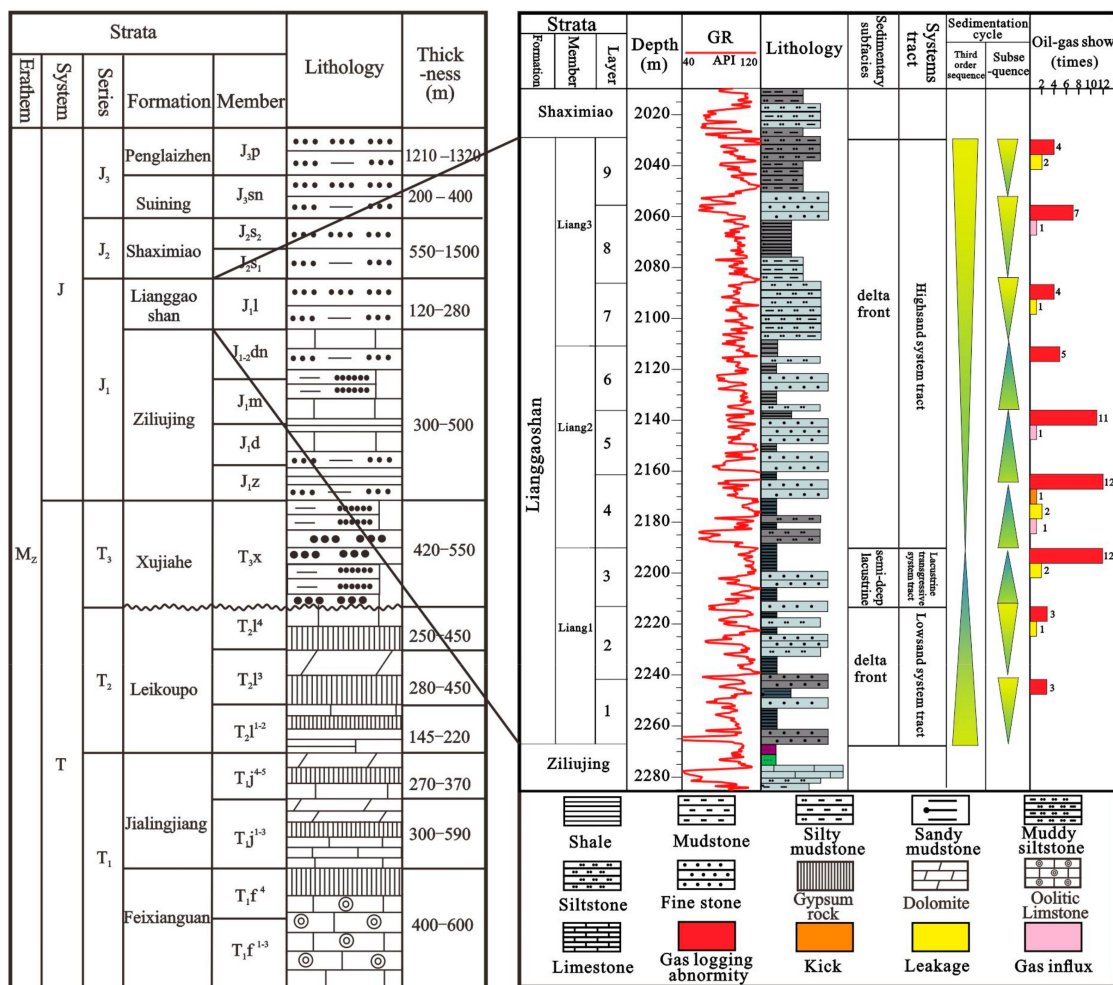

Figure 2. Generalized stratigraphy of the Eastern Sichuan Basin (modified form Li et al., 2015 [31]).

3. Samples and Methods

All of the samples used in this study were taken from conventional cores and from outcrops from the Lianggaoshan Formation in the study area (Table 1). Reservoir pore, petrography and diagenetic events were investigated with the help of thin sections (60 in total), saturated with blue epoxy resin. Alizarin Red S and K-ferricyanide were used to identify different types of carbonate cement. Point counts were performed on thin sections for the content of detrital grains with at least 300 points [32,33].

Table 1. Items and number of experimental analyses in the study.

Experimental Analyses	Number	
	Sandstone	Shale
Thin section	60	/
Scanning electron microscope (SEM)	15	10
Whole rock X-ray diffraction	30	48
Clay mineral X-ray diffraction	9	9
Fluid inclusion analysis	4	/
Porosity and permeability tests	185	92
High-pressure mercury intrusion (HPMI)	5	2
Nuclear magnetic resonance tests (NMR)	5	2

SEM equipped with an energy dispersive spectroscope (EDS) was used to examine authigenic minerals, pore geometry and diagenetic sequence in the 10 shale and 15 sandstone samples. X-ray diffraction (XRD) analysis of whole rock was performed on 30 sandstone and 48 shale core samples with an Ultima IV X-ray diffractometer to identify types and contents of major minerals. The relative contents of different clay of nine sandstone and nine shale core samples were obtained by XRD analysis of quantitative clay minerals. The experimental conditions were 25 °C temperature and 50% humidity. The homogenization temperatures of fluid inclusions was measured in the four sandstone samples by using a petrographical microscope equipped with a Linkam THMSG 600 heating and cooling stage.

The porosity and permeability of 185 sandstone and 92 shale core samples were obtained using conventional physical property tests, and five sandstone and two shale core plugs were conducted for high-pressure mercury intrusion (HPMI) measurements. Afterward, five sandstone and two shale typical samples were selected for the NMR experiment. The pore–throat physical characteristics and distribution in these samples were measured, and the interaction between pore–throat structure and fluid was observed.

4. Results

4.1. Lithological Association

The sand–hale association of Lianggaoshan Formation can be divided into shale dominant type, thin interbed shale-sandstone mixed type and sandstone dominant type according to the vertical combination of sandstone and shale (Figures 2 and 3). The shale dominated type was deposited in the shallow lake and semi-deep lake of layer3 and layer4 (Figures 2 and 3). Shale dominant type, which comprised major shale, argillaceous siltstone and minor siltstone, was characterized by a 10–25 m thickness of shale and less than 1 m of sandstone with, 0–0.2 sand–shale ratio. The shale-sandstone mixed type, which deposited in the distant sand bar and sheet sand of delta front, consists of siltstone and shale with 0.5–2 m of sandstone and 1–2 sand–shale ratio (Figures 2 and 3). Sandstone dominant type was mainly made of fine-grained sandstone and minor thin layer of shale. The sandstone thickness of sandstone dominant type varies from 4 m to 6 m. The sand–shale ratio was generally more than 2 in the sandstone dominant type. Sandstone dominant type was mainly sedimented in the subaqueous distributary channel, and mouth bar of delta front and the layer1, layer6, layer8 and layer9 (Figures 2 and 3).

4.2. Petrography and Mineralogy of Sandstone and Shale

Lianggaoshan Formation sandstones contain detrital components in the following proportions: 34%–60% quartz (ave. 54%), 2%–10% feldspars (ave. 7%), and 10%–47% rock fragments (ave. 40%) (relative content within total detrital grains), dominated by litharenite and a small amount of feldspar lithic sandstone [34] (Figure 4a). The rock fragments are mainly composed of metamorphic rock fragments (80%), volcanic rock fragments (13%), and sedimentary rock fragments (7%) (relative content within total rock fragments) (Figure 5). The detrital feldspars mainly consist of microcline feldspar. The Lianggaoshan Formation sandstones mainly consist of fine-grained, moderate sorted and subangular to subrounded grains (Figure 4b,c). The grain contacts mainly comprise major linear contacts and minor point-linear contacts (Figure 6).

Mineralogy components of Lianggaoshan Formation mudstones are dominated by clay mineral (48%) and quartz (42.2%) (Figure 6). Clay minerals mainly consist of illite/smectite mixed layer, illite, kaolinite, chlorite and chlorite/smectite mixed layer (Figure 6). The brittleness index of Lianggaoshan Formation mudstones mainly varies from 40%–50% with good fracturability (Figure 6).
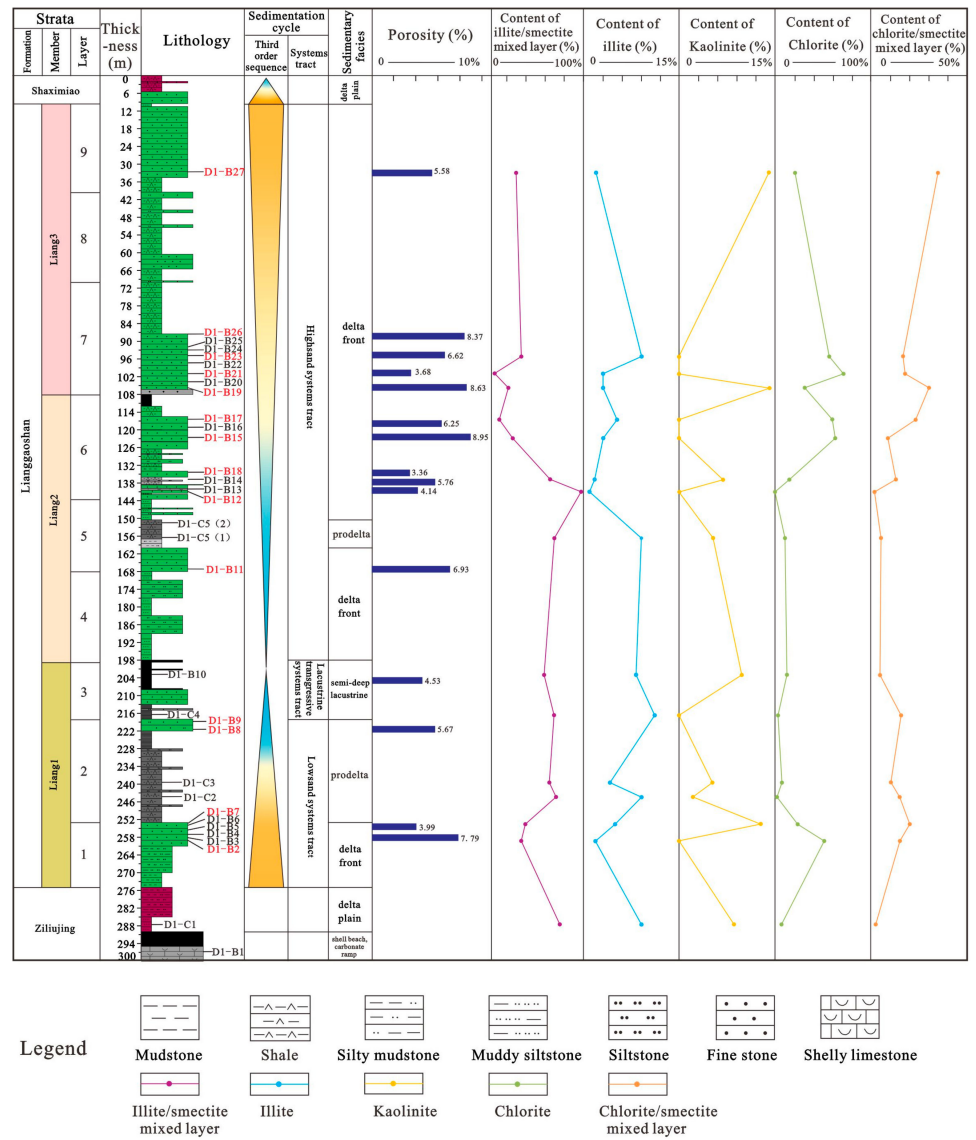
Figure 3. Sequence stratigraph-sedimentary histogram, sample locations, porosity and clay mineral characteristics of Lianggaoshan Formation (Zhangjiawan Section of Wanzhou = ZJW).
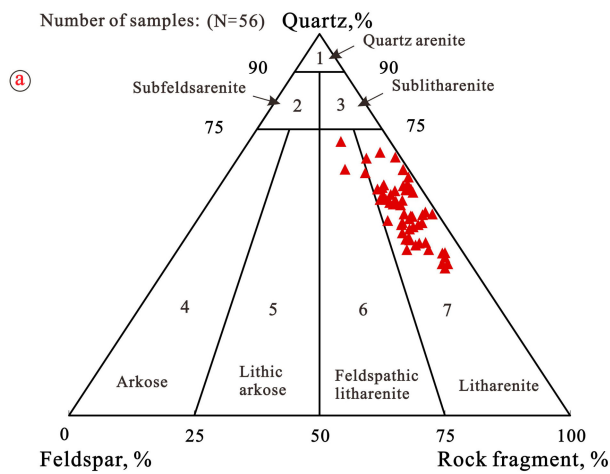

Figure 4. *Cont.*
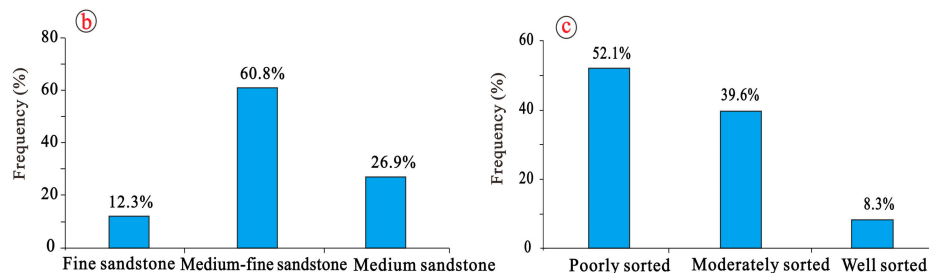
Figure 4. Composition of rock, sorting distribution and lithology of the tight sandstone in Lianggaoshan Formation. (**a**) Classification of sandstone after Folk (1980) classification, (**b**) Lithology distribution, and (**c**) Sorting distribution.
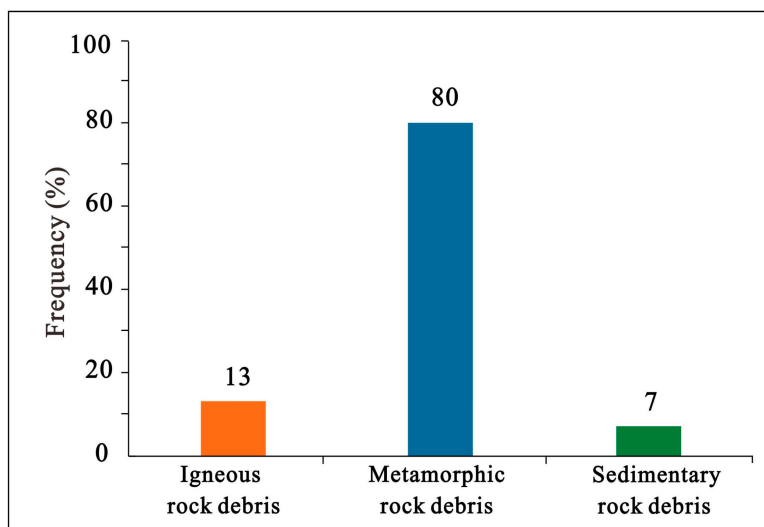

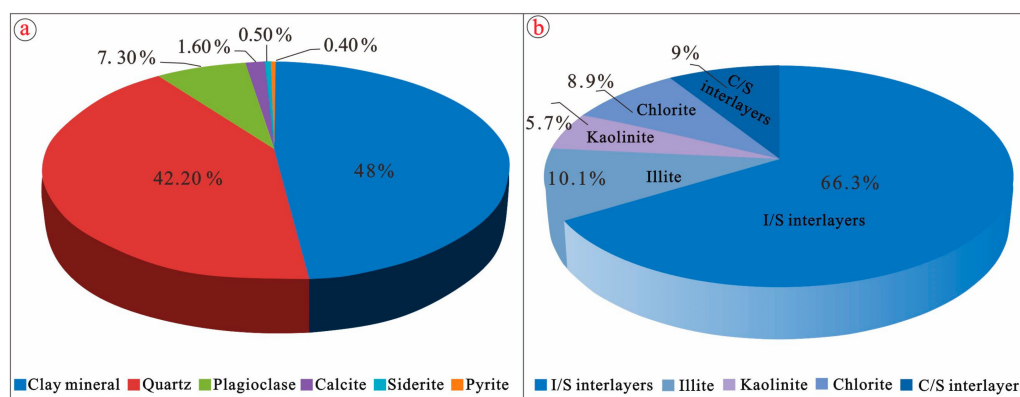**Figure 5.** Type and content of rock fragments of Lianggaoshan tight sandstone.

Figure 6. Mineralogy components of Lianggaoshan Formation shale (**a**) showing the mineralogy components of whole rock; (**b**) showing the types and relative content of clay minerals.

4.3. Diagenetic Minerals and Alterations

4.3.1. Compaction

Framework grains in the Lianggaoshan Formation sandstones are generally heavily compacted, as is evidenced by the linear to concavo-convex grain contacts (Figure 7a), the orientation of the grains, and the deformed and fractured mica and plastic rock fragments. The sutured contacts between quartz grains were rarely observed (Figure 7d). The mechanical compaction is manifested by the directional bent flake clay mineral and micro-fracture in the Lianggaoshan Formation shale (Figure 8).
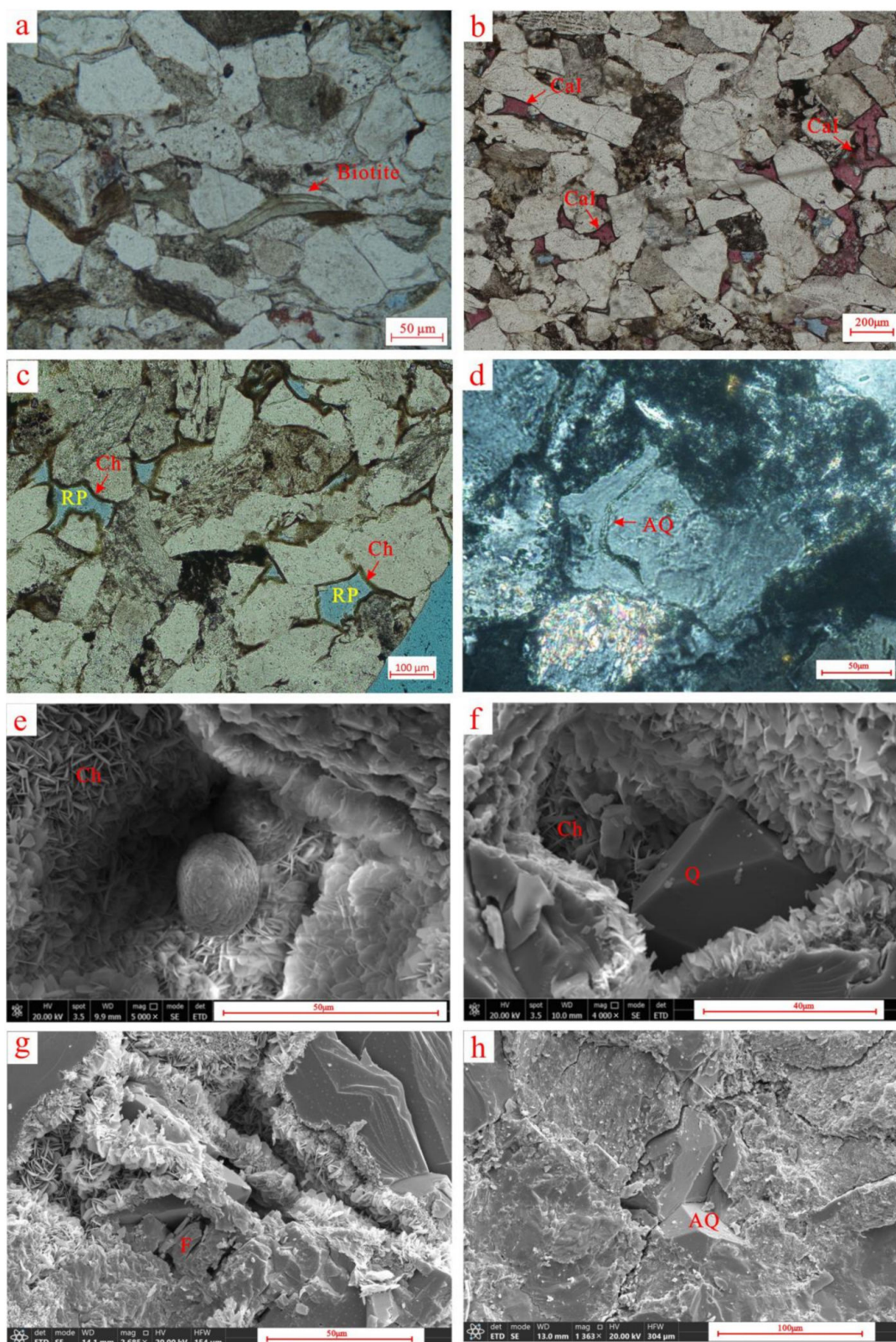
Figure 7. Diagenesis characteristics of Lianggaoshan Formation sandstone in the study area. (**a**) Optical photomicrographs of thin section (XPL) showing linear grain contacts and bending deformation of biotite, medium to fine grained lithic sandstone, Liang1 member (layer1), Zhangjiawan Section. (**b**) Optical photomicrographs of thin section (XPL) showing calcite (cal) filling in pore, medium lithic sandstone, Liang2 member (layer4), Zhangjiawan Section. (**c**) Optical photomicrographs of thin

section (XPL) showing chlorite coats (Ch) and primary pore (RP), medium lithic sandstone, Liang2 member (layer6), Zhangjiawan Section. (**d**) Optical photomicrographs of thin section (XPL) showing quartz overgrowth (AQ), 2158.3 m, (layer5), well YT1; (**e**) SEM image showing residual primary intergranular pore and chlorite coats (Ch), 1764.81 m, (layer8),well ZX1H. (**f**) SEM image showing chlorite coats (Ch), illite and authigenic quartz (Q) in the residual primary intergranular pore, 1813.81 m, (layer8),well ZX1H. (**g**) SEM image showing authigenic quartz (Q) and chlorite coats (Ch) are filled in intergranular pore, and feldspar(F) is dissolved to form dissolution pores, 1793.16 m, (layer8),well TD021-X8. (**h**) SEM image showing quartz overgrowth (AQ); the lamellar chlorite aggregate is attached to the grain surface, and the micro-cracks and dissolution micro-pores between grains are observed, 2014.5 m, (layer8), well YD003-H2.
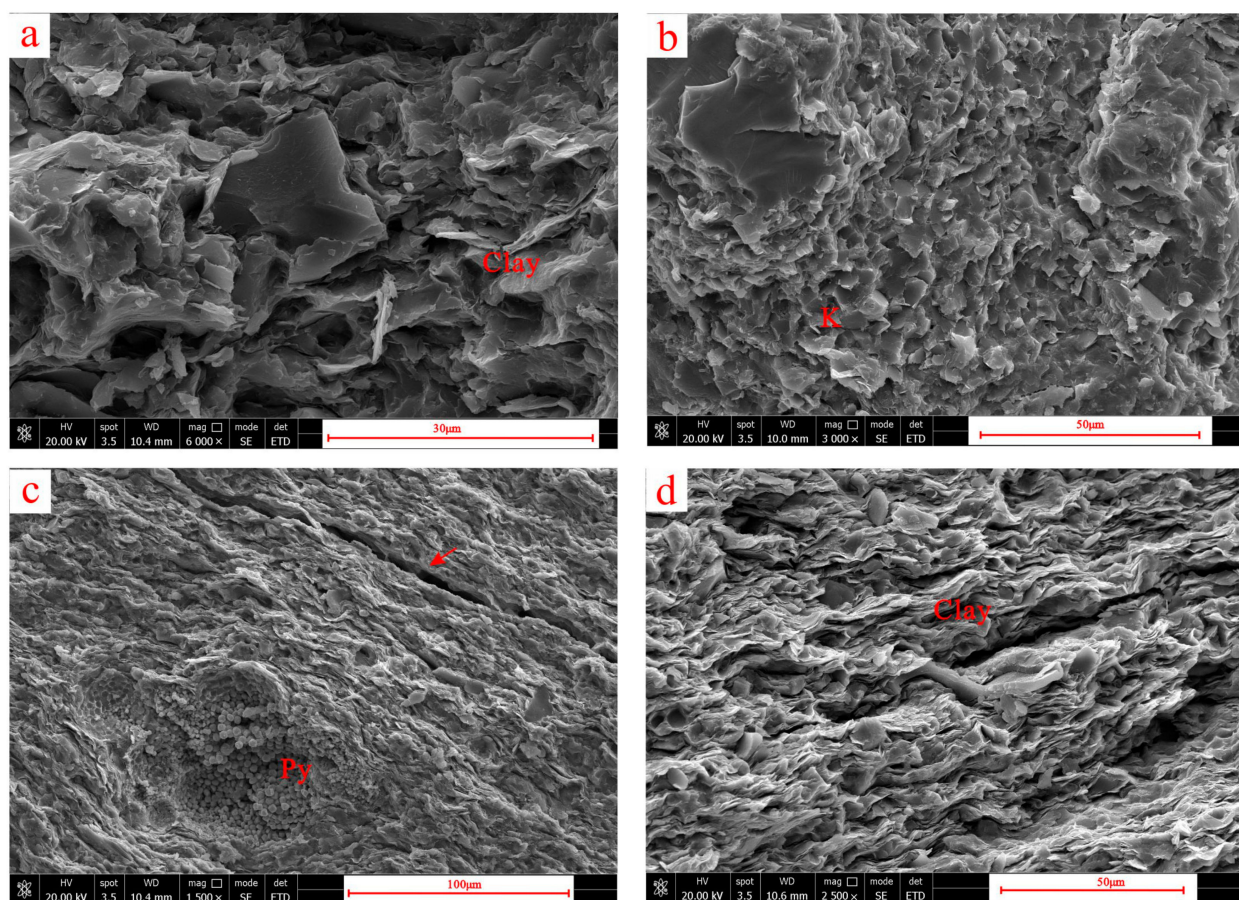

Figure 8. Diagenesis characteristics of Lianggaoshan Formation shale in the study. (**a**) SEM image showing clumpy organic matter and flake clay mineral, 1672.36 m, well DY1. (**b**) SEM image showing authigenic kaolinite (K), 1679.84 m, well DY1. (**c**) SEM image showing directional lamellar clay mineral, authigenic pyrite (Py) and micro fracture in the Lianggaoshan Formation shale, 1686.80 m, well DY1. (**d**) SEM image showing organic matter distributed in the directional lamellar clay mineral, 1690.01 m, well DY1.

4.3.2. Carbonate Cements

Calcite is the primary carbonate cement in the Lianggaoshan Formation sandstones. Its abundance varies from 1 vol% to 11 vol%, with an average of 3.86% (thin-section observation). Carbonate cement occurs either as pore-filling cement and partly replacing feldspar or debris (Figure 7b). Homogenization temperatures of fluid inclusions in calcite cement are mainly distributed in the 100–130 °C and 140–160 °C ranges (Figure 9).
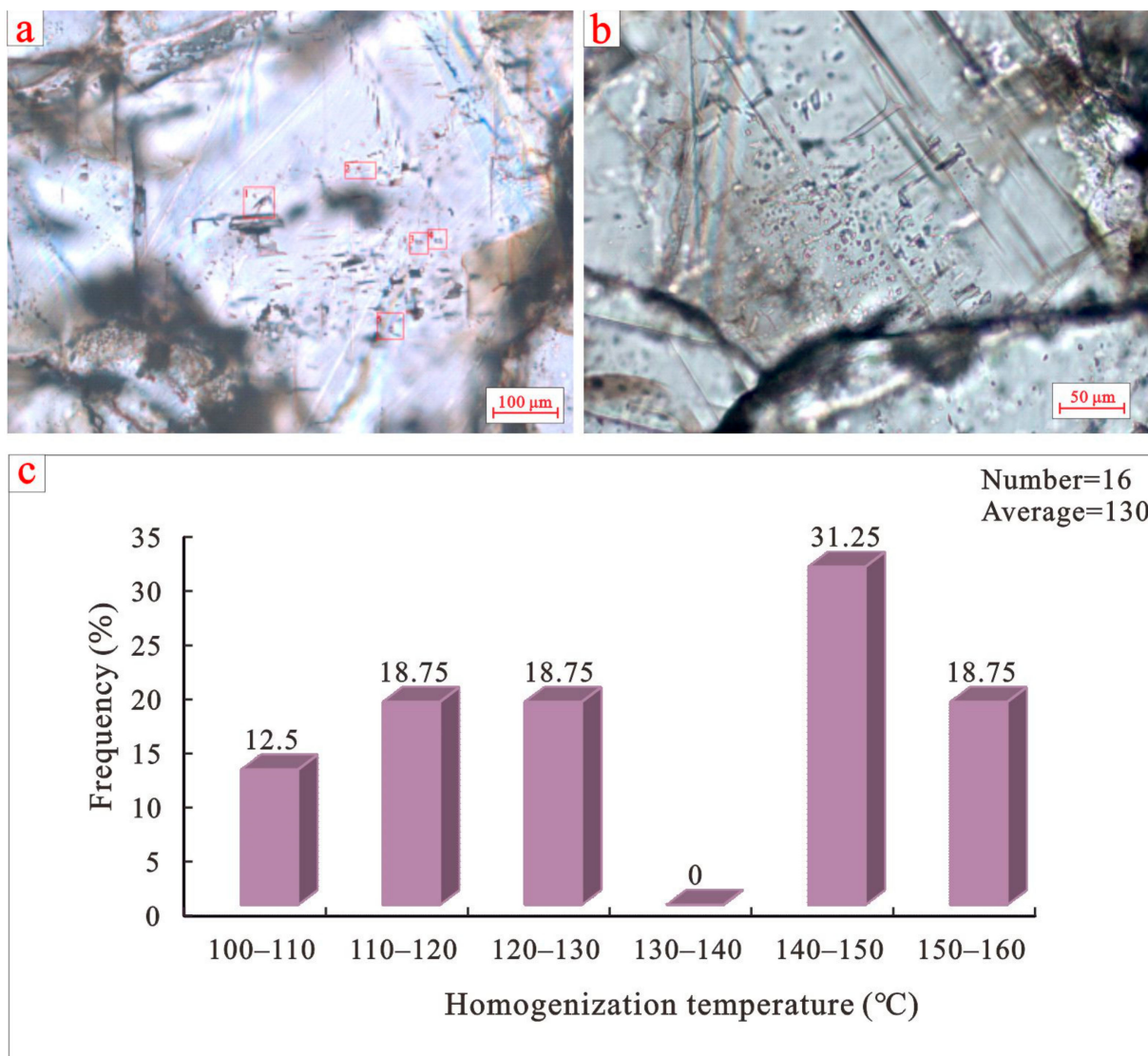
Figure 9. Fluorescence characteristics and homogenization temperature of fluid inclusions within the calcite cement. (**a**,**b**) showing the fluid inclusion photograph under the microscope. (**c**) showing the distribution of homogenization temperature of fluid inclusions within the calcite cement.

4.3.3. Quartz Overgrowth

Quartz cement in the form of quartz overgrowths (Figure 7d) occurs around detrital quartz grains and the pore-filling quartz (Figure 7f). Authigenic quartz generally co-occurs with partially dissolved feldspars and rock fragment dissolution (Figure 7g). Pore-filling quartz cements have also been observed (Figure 7h).

4.3.4. Clay Minerals

The total clay mineral content varies from 9% to 38% (mass fraction), with an average of 20.4% (mass fraction), in the Lianggaoshan sandstones (Table S1). Authigenic clay minerals comprise kaolinite, chlorite, illite, illite/smectite mixed layer and chlorite/smectite mixed layer in the Lianggaoshan sandstones (Table S1). Chlorite, which was mainly developed in the branch channel sandstone, occurs as pore-filling chlorite and chlorite coat (Figure 7c,e). Chlorite coat generally occurs together with primary intergranular pores (Figure 7c,e). Both chlorite content in the clay mineral and the chlorite coat increases with increasing distance to the interface of sandstone and mudstone (Figure 10a,b).
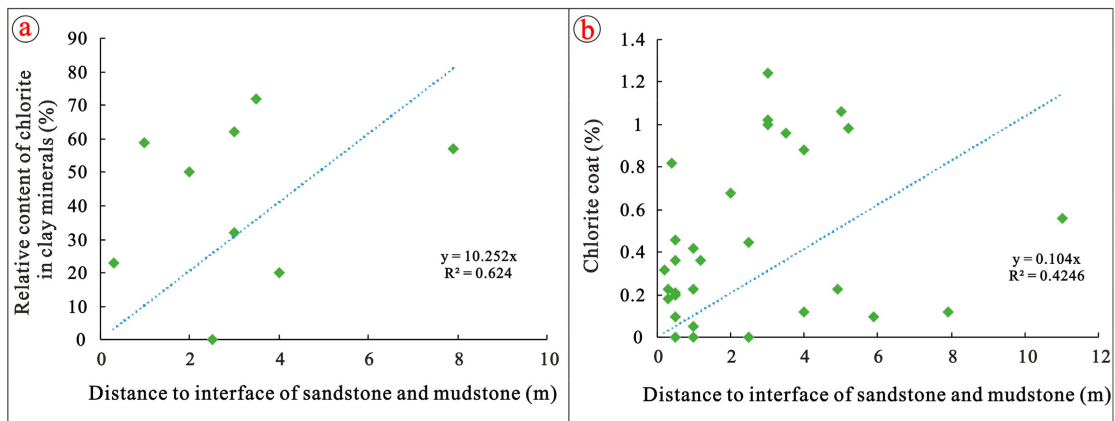
Figure 10. The relationship between chlorite coat within sandstone and interface of sandstone and mudstone in the Lianggaoshan Formation study area. (**a**) showing the relationship between the relative content of chlorite coat within sandstone and distance to interface of sandstone and mudstone (Data from XRD analysis). (**b**) showing the relationship between absolute content of chlorite coat within sandstone and distance to interface of sandstone and mudstone (data from thin section).

4.3.5. Dissolution

Feldspar including plagioclase and orthoclase was partially or totally dissolved. Secondary pores, which were generally formed by the feldspar dissolution and some calcite dissolution, were mainly developed in the interface of sandstone and shale (Figures 3, 7g and 11a).
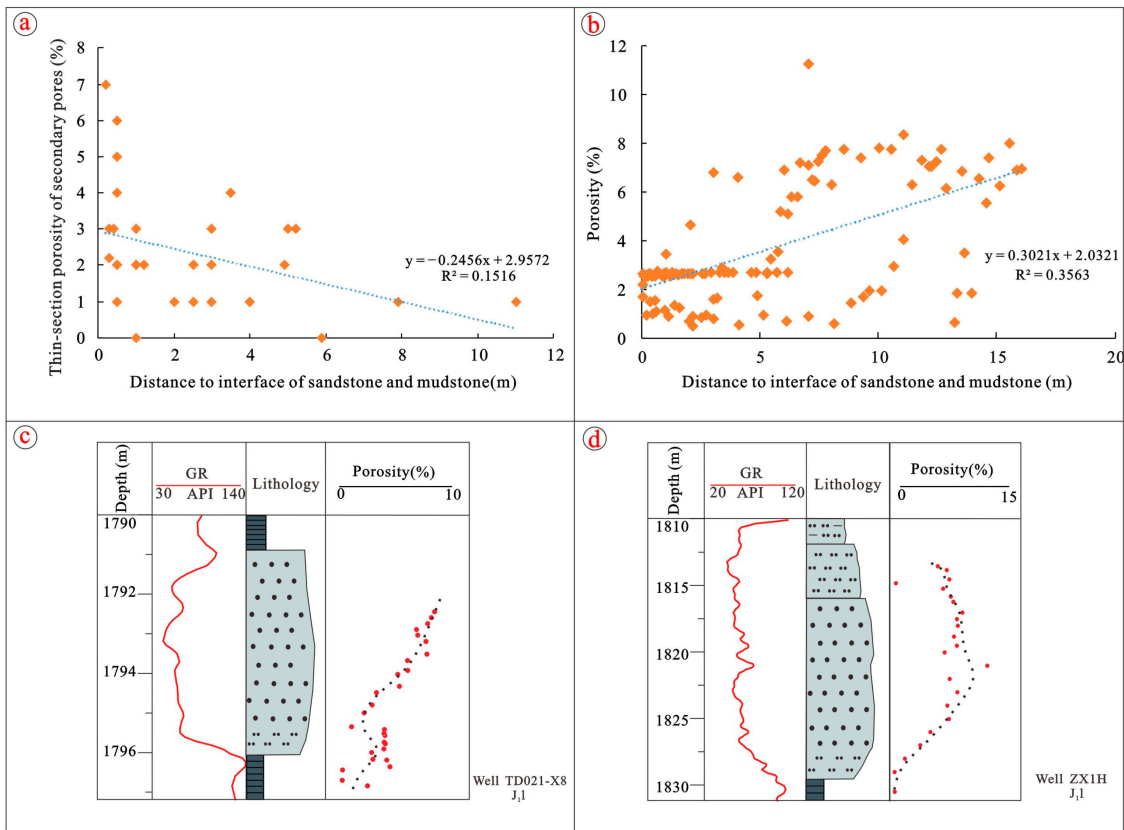

Figure 11. The relationship between sandstone porosity ((**a**) represents thin-section porosity, (**b**) represents the measure porosity) and interface of sandstone and mudstone in the Lianggaoshan Formation study area. Porosity profiles of representative sandstones from wells TD021-X8 (**c**) and ZX1H (**d**).

4.4. Geochemistry of Sandstone and Shale

The thickness of Lianggaoshan Formation dark shale mainly varies from 30 m to 65 m in the study area. Dark shale was mainly developed in the layer3 and was one of the most important source rocks in the Lianggaoshan Formation study area (Figures 2 and 3). The total organic carbon (TOC) content of layer3 dark shale ranges from 0.49% to 2.85%, with an average value of 1.34% (Figure 12). The vitrinite reflectance of the drilling core shale varies from 1.0% to 1.29% (Table 2; Figure 12). The vitrinite reflectance of the outcrop shale varies from 0.62% to 0.95% (Table 2). The kerogens of Lianggaoshan Formation shale belong to the Type II with minor Type III [35].
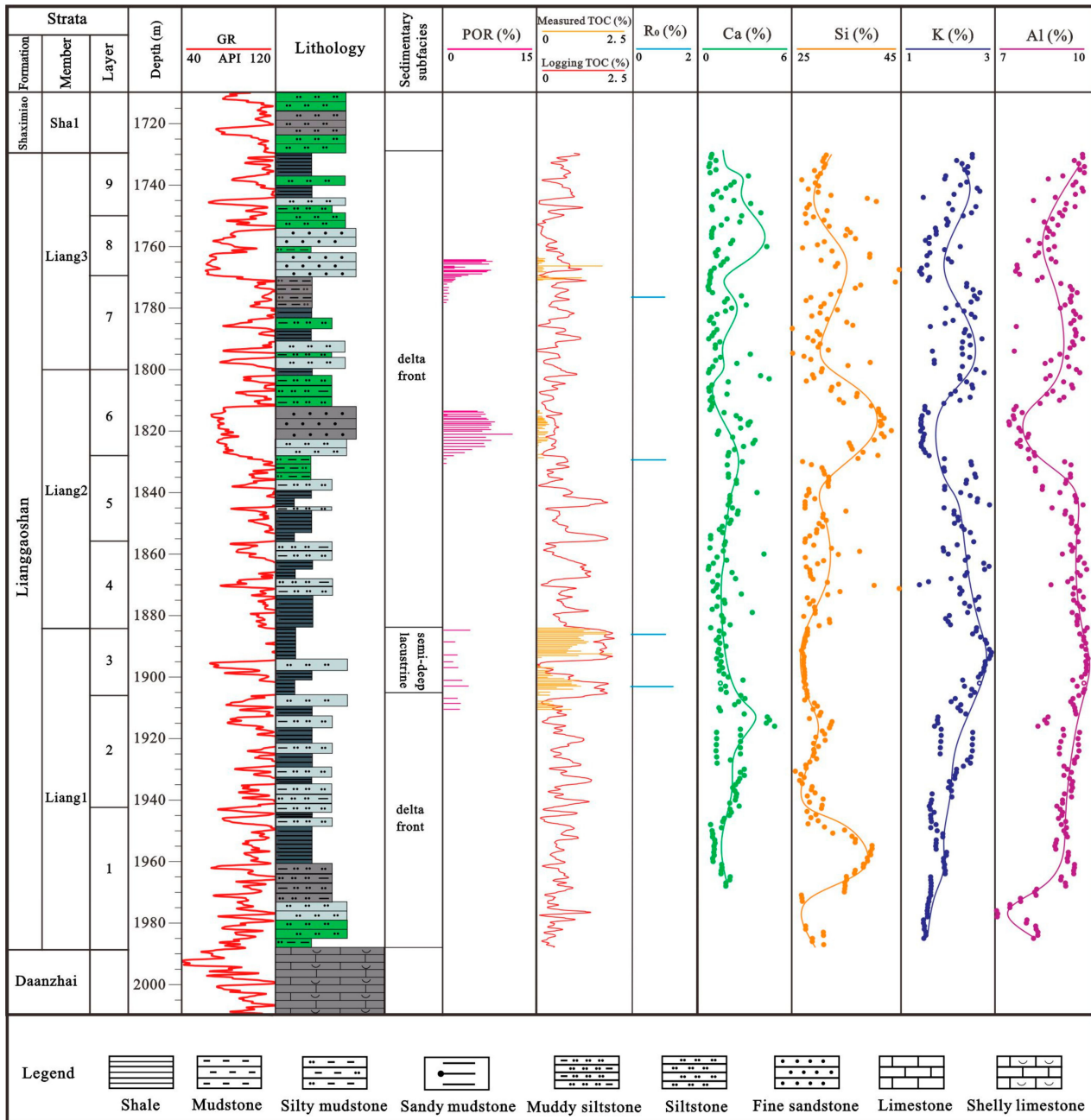

Figure 12. The lithology, porosity and major elements of the Lianggaoshan Formation in well ZX1 of the study area.

**Table 2.** Vitrinite reflectance (R_O) of the Lianggaoshan Formation shale.

Sample	Depth (m)	Sample Type	Strata	Lithology	R_O%
D2-C2	96	Outcrop	layer3	Gray-black shale	0.62
D3-C1	114	Outcrop	layer4	Gray black shale	0.73
D4-C2	133	Outcrop	layer5	Gray black shale	0.95
ZX1H	1776.4	Core	layer7	Dark gray argillaceous siltstone	1.02
ZX1H	1828.7	Core	layer6	Gray black silty shale	1.09
ZX1H	1887.5	Core	layer3	Black shale	1.1
ZX1H	1902.1	Core	layer3	Black shale	1.29

The elemental logging indicates that the calcium (Ca) content is low in the shale (e.g., layer3) and high in the sandstone (e.g., layer2, layer6 and layer8) (Figure 12). The content of calcium (Ca) in center of a sandstone body is generally less than in the interface of sandstone and shale (Figure 12).

The elemental logging indicates that the silicon (Si) content is high at the interface of sandstone and shale (layer1 and layer8) (Figure 12). The elemental logging indicates that the potassium (K) element and the aluminum (Al) are abundant in the shale (e.g., layer3) and have low abundance in the sandstone (e.g., layer6 and layer8) (Figure 12). The content of aluminum (Al) co-varies with potassium (K) (Figure 12). The aluminum (Al) content of sandstone and shale is almost consistent from layer1 to layer5 and reaches a maximum value in the layer3 (Figure 12). Silicon is enriched in the sandstone relative to the shale (Figure 12).

4.5. Types and Structure of Pore Space

The pore types of the Lianggaoshan sandstones mainly consist of residual primary intergranular pores, intergranular dissolved pores and intragranular dissolution pores in the study area (Figures 7b,c,e,f, 13 and 14), some residual primary intergranular pores that are coated by chlorite films (Figure 14a,c), and secondary pores, which consist of intergranular dissolution pores, intragranular dissolution pores, small amounts of moldic pores and fractures (Figures 13 and 14b,c). The intergranular dissolution pores were generally derived from the part dissolution of feldspars and pore-filling calcite cement (Figure 14b,c). In addition, the intragranular pores were generally formed from the partial to complete dissolution of feldspar and some rock fragments (Figure 14b).
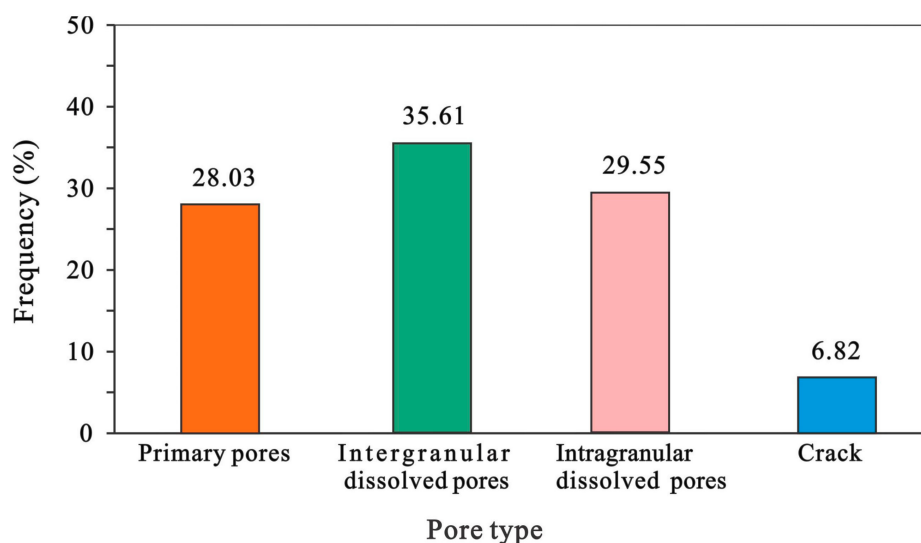
Figure 13. Frequency distribution of pore types in the Lianggaoshan Formation sandstones of the study area (based on the point counts).
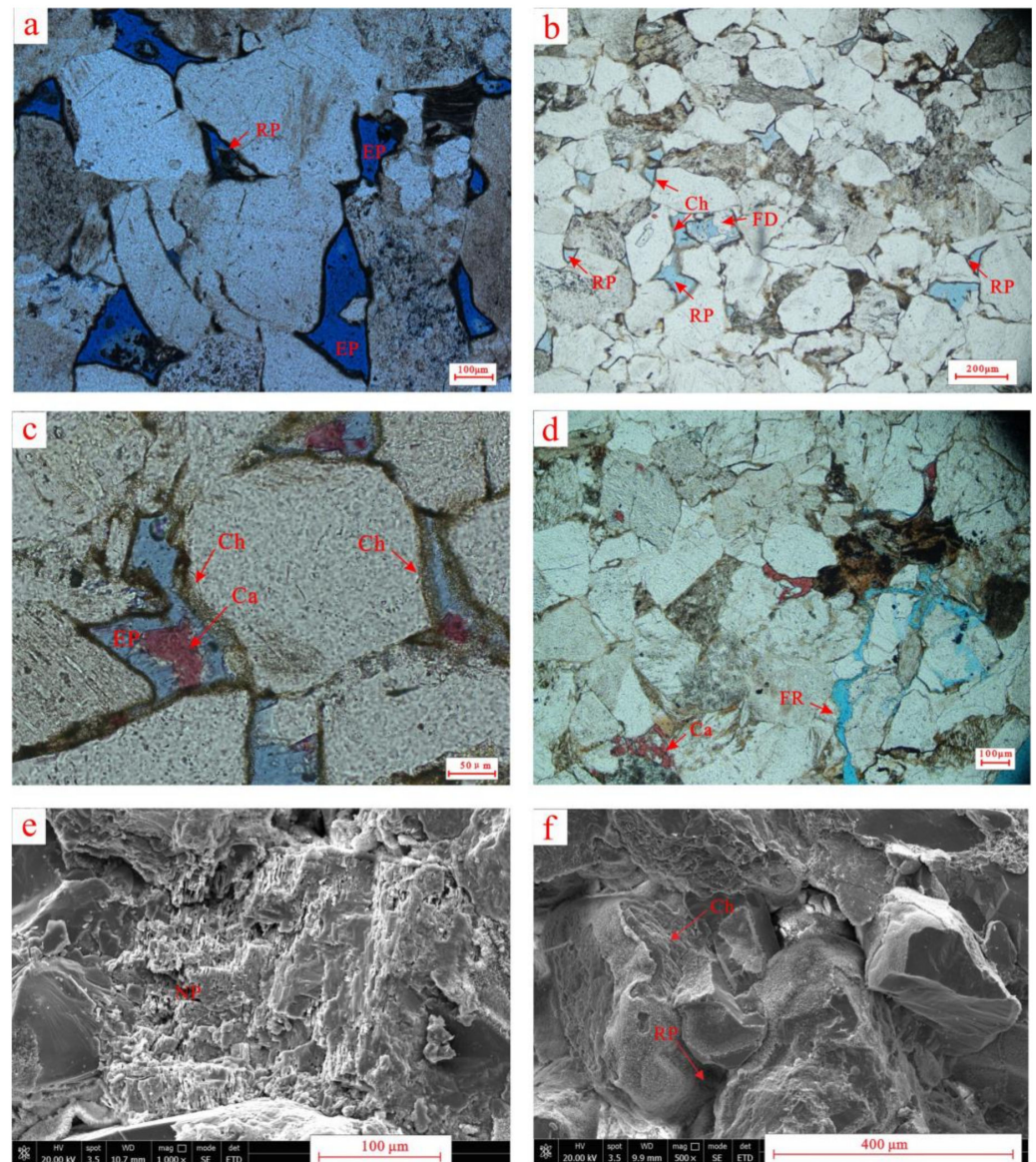
Figure 14. Types and characteristics of pore space of the Lianggaoshan Formation tight sandstone in study area. (**a**) Optical photomicrographs of thin section (XPL) showing primary intergranular pores (RP) and intergranular (EP) dissolved pores, Well ZX1H, 1764.36 m, J₁l. (**b**) Optical photomicrographs of thin section (XPL) showing primary intergranular pores (RP) and intragranular (NP) dissolved pores of feldspar (FD), Zhangjiawan, 170.5 m, J₁l. (**c**) Optical photomicrographs of thin section (XPL) showing that the pore filling calcite (Ca) cement and primary pores (RP) was surrounded by chlorite coating (Ch), Zhangjiawan, 170.5 m, J₁l. (**d**) Optical photomicrographs of thin section (XPL) showing the pore (NP) filling calcite (Ca) cement and fracture (FR), Jiangyincun, 104.7 m, J₁l. (**e**) SEM image showing intergranular (EP) dissolved pores in the feldspar, ZX1H, 1764.81 m, J₁l. (**f**) SEM image showing that primary intergranular pores (RP) were surrounded by chlorite coating, ZX1H, 1764.81 m, J₁l.

The pore types of the Lianggaoshan Formation shale mainly include intergranular dissolution pores, intercrystal pores and micro-fractures in the study area. The asphalt was generally distributed in the intergranular dissolution pores, intercrystal pores (clay mineral or pyrite) and micro-fractures (Figure 15).
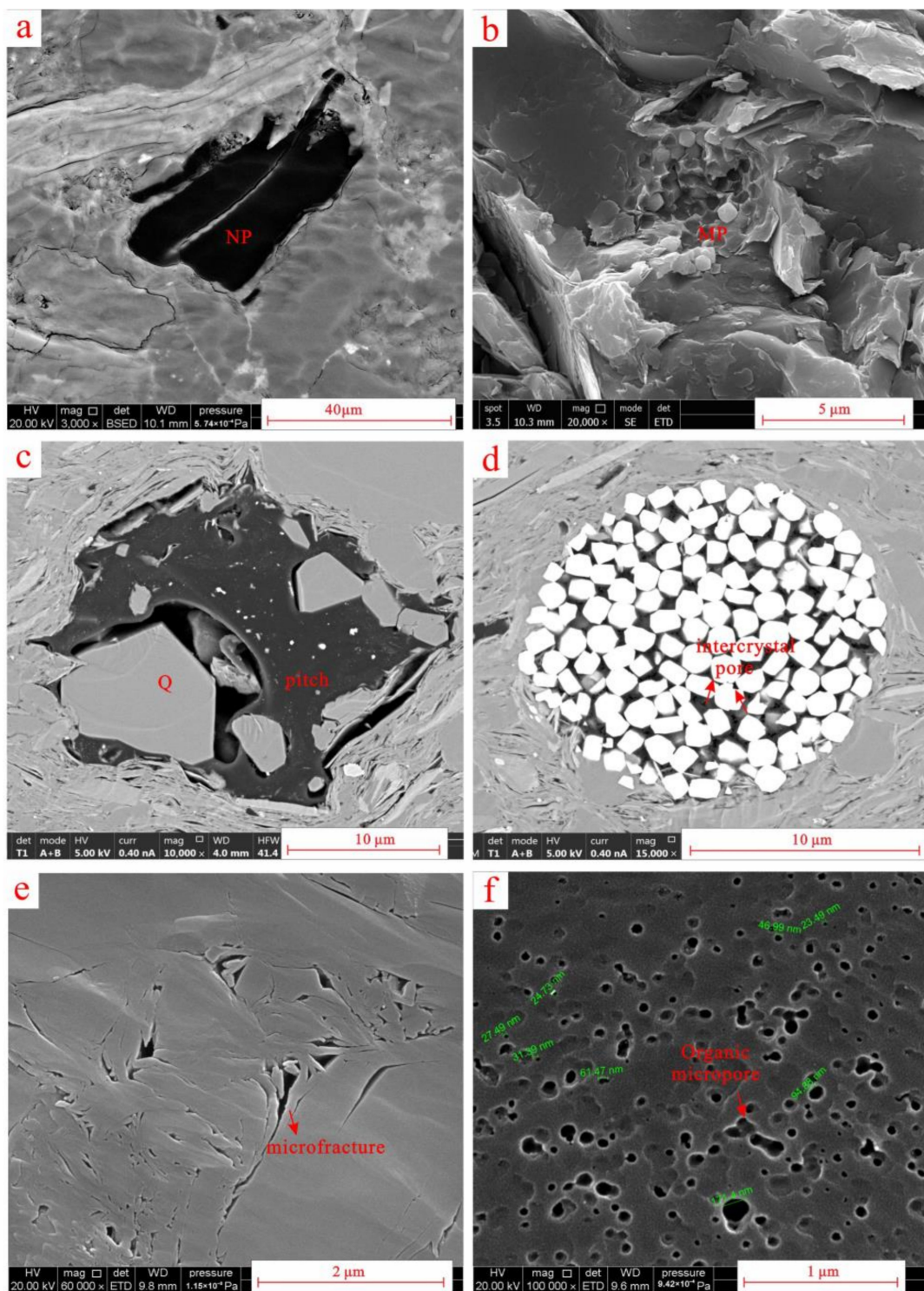
Figure 15. Types and characteristics of pore space of the Lianggaoshan Formation shale in the study area. (**a**) SEM image showing intragranular (NP) dissolved pores filled with organic matter, Zhangjiawan shale, 257 m, layer1. (**b**) SEM image showing pyrite and the moldic pore (MP) caused by fall out of pyrite, well DY1, 1683.72 m, layer3. (**c**) SEM image showing shale pore filled with quartz and pitch, 2161.42 m, layer5. (**d**) SEM image showing intercrystal pore of globular pyrite filled with pitch, 2161.42, layer5. (**e**) SEM image showing intercrystal pore of clay mineral and microfracture, Zhangjiawan shale, 202.5 m, layer3. (**f**) SEM image showing organic micropores, Zhangjiawan shale, 244 m, layer2.

The maximum pore throat radius of Lianggaoshan Formation sandstone varies from 0.134 to 0.358 μm (Figures 16 and 17). The average pore throat radius of Lianggaoshan Formation sandstone ranges from 0.036 to 0.090 μm (Figures 16 and 17). The pore throat is characterized by multimodal distribution.
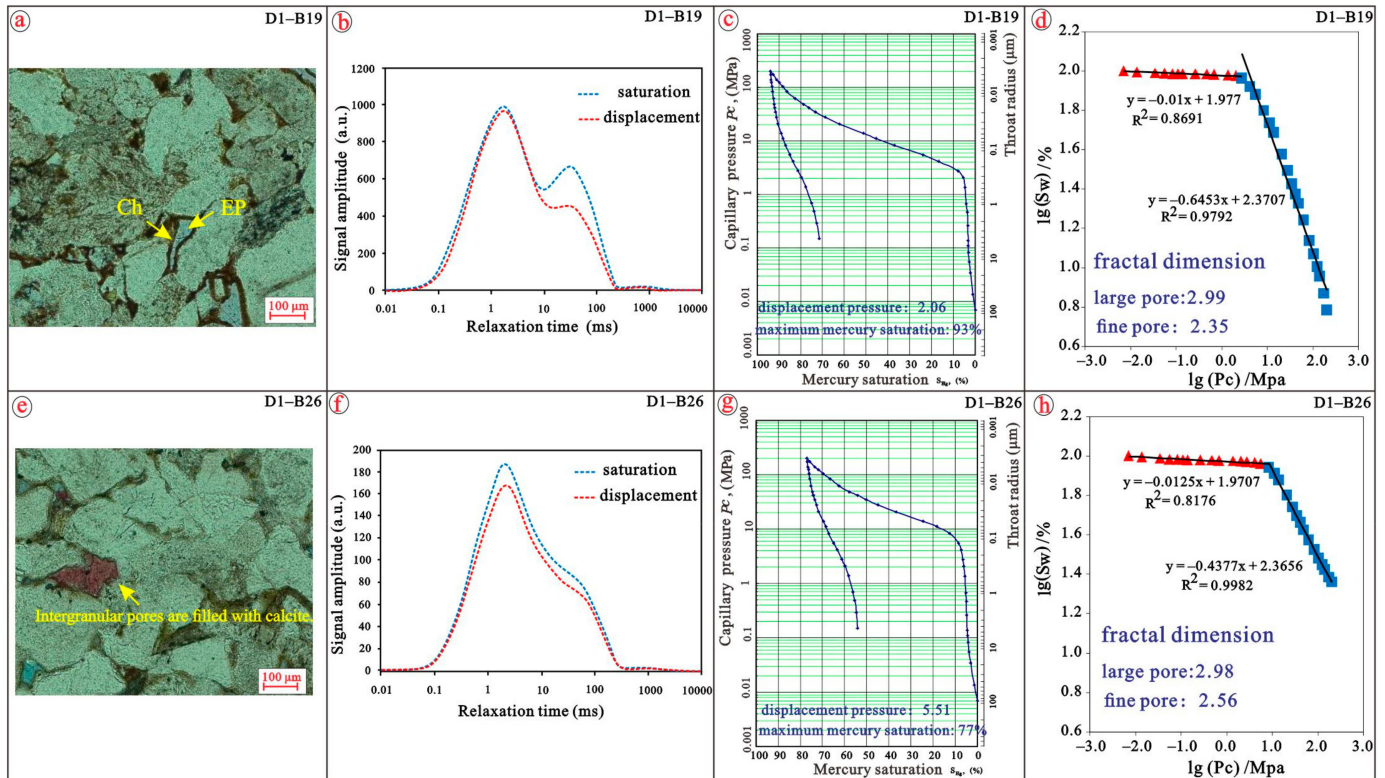

Figure 16. Characteristics of pore structure in the Lianggaoshan Formation sandstone of study area22. The sandstone (D1–B19, Zhangjiawan section) rich in chlorite coat is characterized by abundant primary pores (**a**), big pores (**b**), low displacement pressure and high saturation of mercury intake (**c**), weak complexity of pore-throat (**d**). The sandstone (D1–B26, Zhangjiawan section) rich in chlorite coat and pore-filling calcite is characterized by medium primary pores (**e**), some big pores and small pores (**f**), high displacement pressure and low saturation of mercury intake (**g**), poor connectivity of pore-throat (**h**). EP = primary pore, Ch = chlorite coat.

Some sandstone beds (CC sandstone) are rich in chlorite grain coats in the Lianggaoshan Formation in the study area (Figure 16a). Pore space of CC sandstone mainly comprises primary pores and minor secondary pores (Figure 16a) and consists of big pores and small pores in CC sandstone (Figure 16b). CC sandstone is characterized by low displacement pressure (2.06 MPa) and high saturation of mercury intake (93%) (Figure 16c), 2.99 fractal dimension of big pores and 2.35 fractal dimension of small pores (Figure 16d). The intergranular pores of some sandstones (CCA sandstone) are generally surrounded by chlorite coat and filled with pore-filling calcite (Figure 16e). The CCA sandstone is characterized by some big and small residual primary pores (f) with high displacement pressure (5.51 MPa) and low saturation of mercury intake (93%) (Figure 16g), and poor connectivity of pore-throat (Figure 16h). Some sandstone (LC sandstone) was lake of chlorite coat and primary pores (Figure 17a,e). LC sandstone was characterized by linear contacts (Figure 17a,e), moderate displacement pressure (Figure 17b,f), high saturation of mercury intake (Figure 17c,g) and poor connectivity of pore-throat (Figure 17d,h).
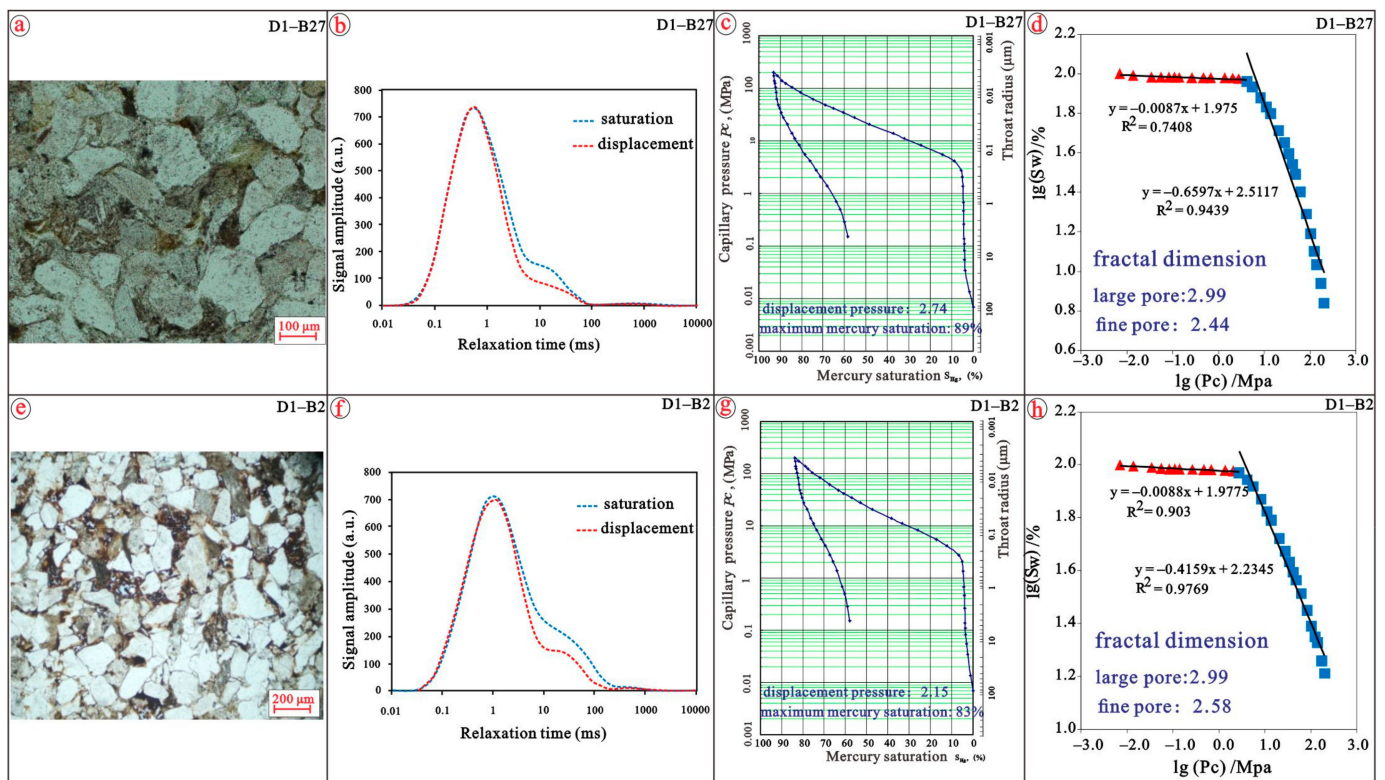
Figure 17. Characteristics of pore structure in the Lianggaoshan Formation sandstone of study area22. The sandstone (D1–B27, Zhangjiawan section) poor in chlorite coat and pore-filling calcite is characterized by secondary pores (**a**), small pores (**b**), medium displacement pressure and saturation of mercury intake (**c**), poor connectivity of pore-throat (**d**). The sandstone (D1–B26, Zhangjiawan section) with small amount of chlorite coat is characterized by some primary pores (**e**), small pores and few big pores (**f**), low displacement pressure and high saturation of mercury intake (**g**), poor connectivity of pore-throat (**h**).

4.6. Porosity and Permeability

Conventional core analysis of 185 samples from the Lianggaoshan sandstones shows that the sandstones have porosities that range from 0.35% to 11.24%, with an average of 3.61% (Figure 18a), and the core permeability ranges from 0.001 to 1 mD, with an arithmetic average of 0.017 mD (Figure 18c). The porosity of Lianggaoshan Formation shale mainly varies from 1.44% to 4.99%, with an average of 2.28% (Figure 18b). Permeability of the Lianggaoshan Formation shale is generally less than 0.01 mD, with an average of 0.007 mD (Figure 18d). The Lianggaoshan sandstones and shale belong to low-porosity and low-permeability tight reservoirs with poor correlations between porosity and permeability (Figure 18e,f).The porosity increases with increasing distance from the interface of sandstone and mudstone (Figure 11b–d). The porosity of sandstone in layer6, layer7 and layer8 of the highstand system tract was usually higher than that of the sandstone of other layers in the lowstand system tract and lake transgression system tract (Figures 2 and 3).
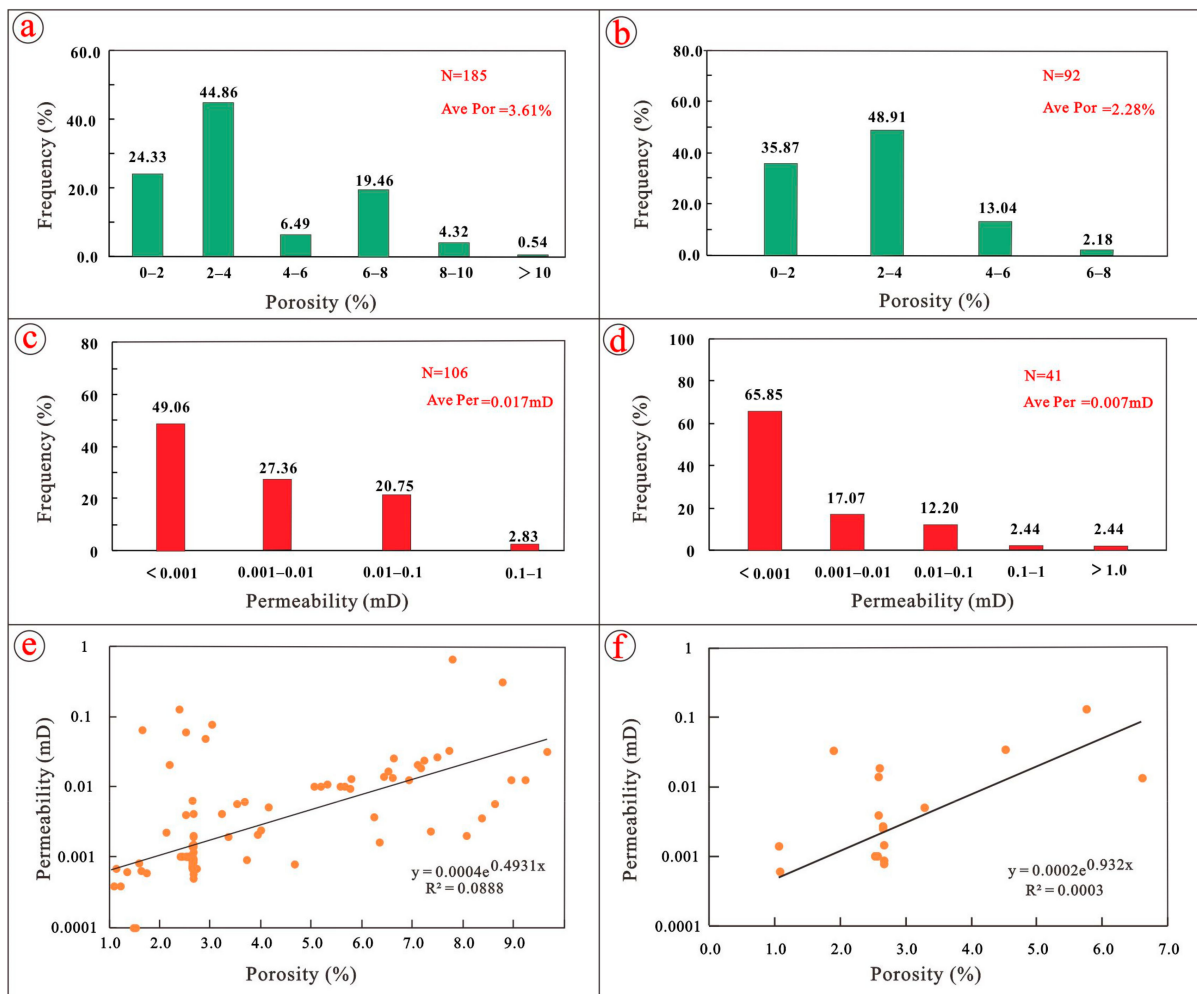
Figure 18. Distribution characteristics of porosity and permeability in the Lianggaoshan Formation sandstone and shale of study area. (**a**) showing the distribution of porosity in the Lianggaoshan Formation sandstone; (**b**) showing the distribution of porosity in the Lianggaoshan Formation shale; (**c**) showing the distribution of permeability in the Lianggaoshan Formation sandstone; (**d**) showing the distribution of permeability in the Lianggaoshan Formation shale; (**e**) showing the relationship between the porosity and permeability in the Lianggaoshan Formation sandstone; (**f**) showing the relationship between the porosity and permeability in the Lianggaoshan Formation shale.

5. Discussion

5.1. Diagenetic Sequence of Sandstone

The burial depth of the Lianggaoshan Formation varies from 1700 to 2000 m. The vitrinite reflectance of the Lianggaoshan Formation shale almost reaches 1.29% in the well, and the ratio of smectite in the mixed layer mainly ranges from 5%–10% (Supplementary File). These indicate that Lianggaoshan Formation sandstone and shale were at the mesodiagenesis stage (Figure 19). The relative diagenetic sequence of Lianggaoshan Formation sandstone was revealed by the petrographic evidence from thin-section and electron microscope (SEM) analysis in the study area. The occurrence sequence of main diagenetic events was mechanical compaction, authigenic chlorite coat (rim)—calcite cementation-dissolution-quartz cement-kaolinization-illitization (Figure 19). The diagenetic evolution sequence of Lianggaoshan Formation sandstone, in which the burial and thermal histories are based on the results of previous studies 22, was illustrated on the basis of the burial and thermal histories of previous studies (Figure 19).
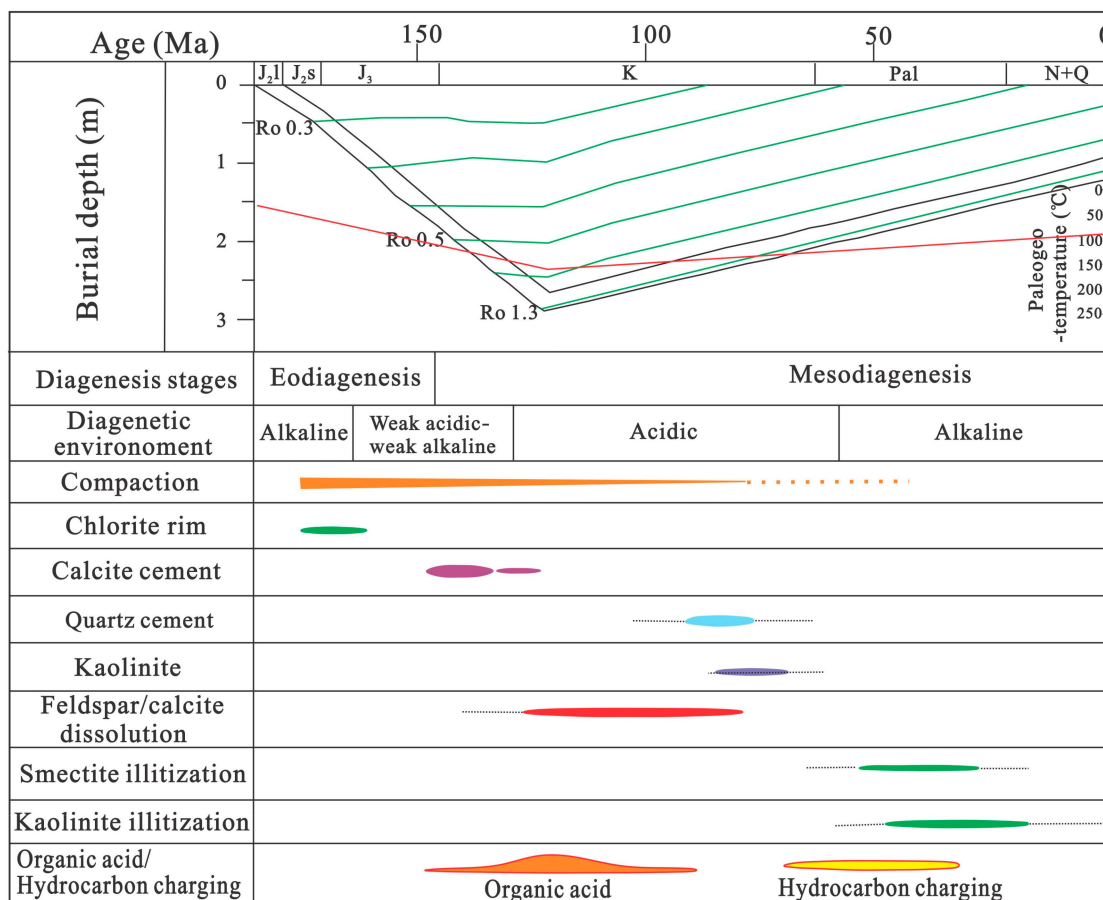
Figure 19. Diagenetic sequence, burial and thermal history of Lianggaoshan Formation in the study area [36].

5.2. Thermal Evolution of Source Rock

Oil and gas shows, lithology and total organic carbon (TOC) content indicate that dark shale of the layer3 was the most important petroleum source rock within the Lianggaoshan Formation (Figures 2, 3 and 12, Table 2). The Lianggaoshan Formation shale reached mature—high mature stage in the study area as indicated by the vitrinite reflectance (Ro) ranging from 1.0% to 1.29% (Figure 12, Table 2). The organic acid formation was mainly related with the total organic carbon (TOC), vitrinite reflectance (Ro) and kerogen type of mudstone [14,37–39]. The production rate of organic acid of Type III kerogen is generally higher than that of Type I and Type II kerogen under the same maturity conditions [14,39]. Some kerogen started to generate organic acids (amino acids, fulvic acids and humic acids) when the vitrinite reflectance (Ro) was lower than 0.5 in the mudstone [14,37] (Figure 20). Kerogen generated abundant organic acid (carboxylic acid) and a small amount of hydrocarbon at the early stage of mesodiagenesis, when the vitrinite reflectance (Ro) was higher than 0.5 [14,37] (Figure 20). The organic acid of source rock was mainly formed between 80–120 °C [37].

Lianggaoshan Formation shale reached mature—high maturity stage in the study area, because the vitrinite reflectance (Ro) ranges from 1.0% to 1.29% (Figure 12, Table 2). Therefore, the Lianggaoshan Formation source rock started to generate organic acids (amino acids, fulvic acids and humic acids) at the eodiagenesis stage [14,37]. Then, the Lianggaoshan Formation source rock, which comprises Type II and minor Type III of kerogen, started to generate abundant organic acid (carboxylic acid) during the deposition of the Shaximiao Formation (170 Ma) [37,40] (Figures 19 and 20). The kerogen usually starts to enter the hydrocarbon generation peak when the formation temperature is higher than 120 °C [14,37]. There are more oil and gas shows in the layer3 and layer4 than

in other layers (Figure 2). Therefore, the Lianggaoshan Formation source rock (layer3) started to produce abundant hydrocarbon and some acids in the early Cretaceous period (1.0% < Ro < 1.3%) [14,37,41] (Figures 19 and 20).

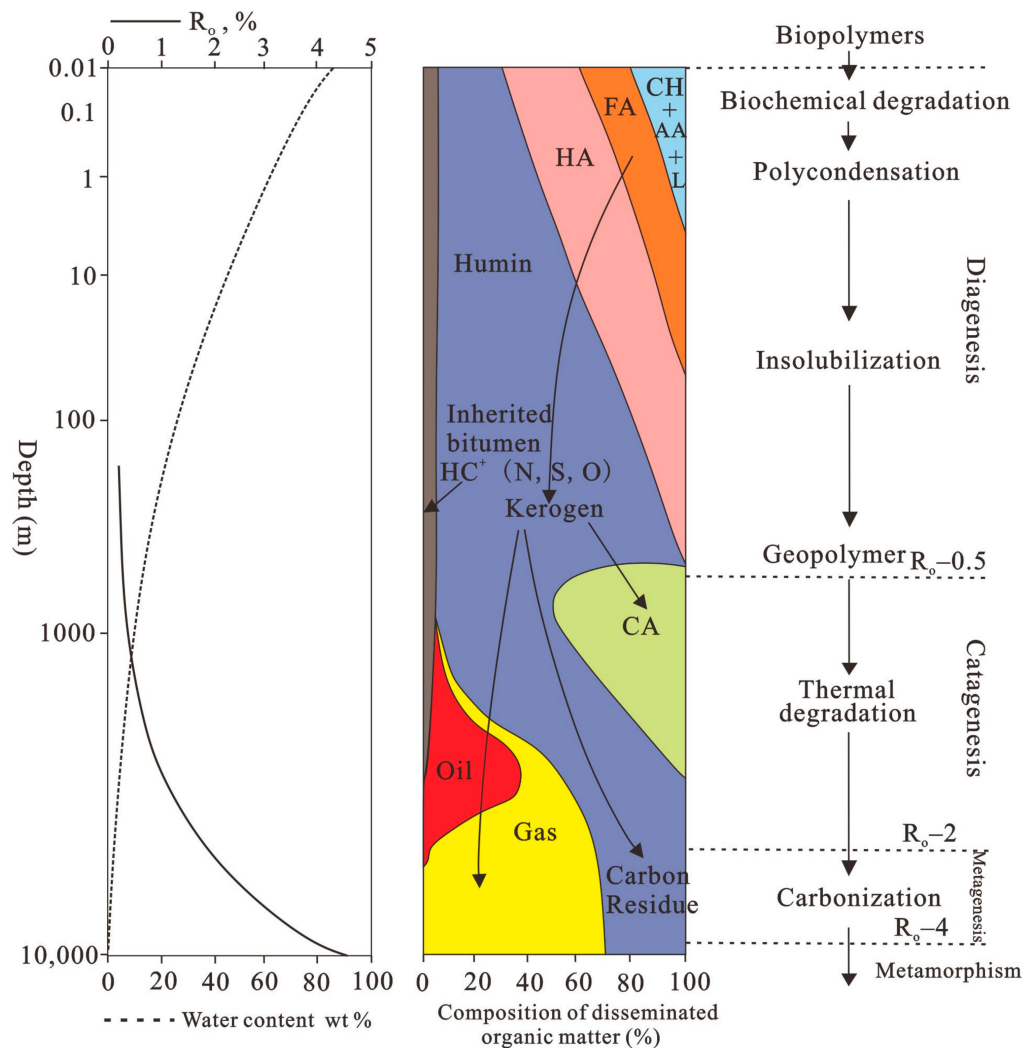**Figure 20.** Thermal evolutionary progress of organic matter in the mudstone (Surdam et al., 1989 [37]).

5.3. Mass Transfer in the Diagenetic System of Tight Sandstone-Shale

The primary porosity of shale is generally higher than that of sandstone, so that the abundant porewater within shale will enter sandstone due to the differential compaction during eodiagenesis [42,43]. The abundant Ca^{2+} and CO_3^{2-} can be released into porewater by organic acidic dissolution due to thermal evolution in the source rock [37,40,44,45]. The calcite cement content decreases with increasing distance to the interface of sandstone and shale (Figure 21a). Calcium (Ca) element content in the shale is generally less than that in sandstone (Figure 12). Moreover, calcium (Ca) element is more enriched in the center of the sandstone body than at the interface of sandstone and shale (Figure 12). These can be interpreted as indicating that the pore water with high concentration of Ca^{2+} and CO_3^{2-} entered the sandstone reservoir due to the shale compaction [42] (Figure 22). There are more oil and gas shows in the layer3, layer4 and layer5 than in other layers (Figure 2). Therefore, the calcite cement preferentially precipitated at the boundary of sandstone compared with the center of sandstone [46] (Figures 21a and 22).
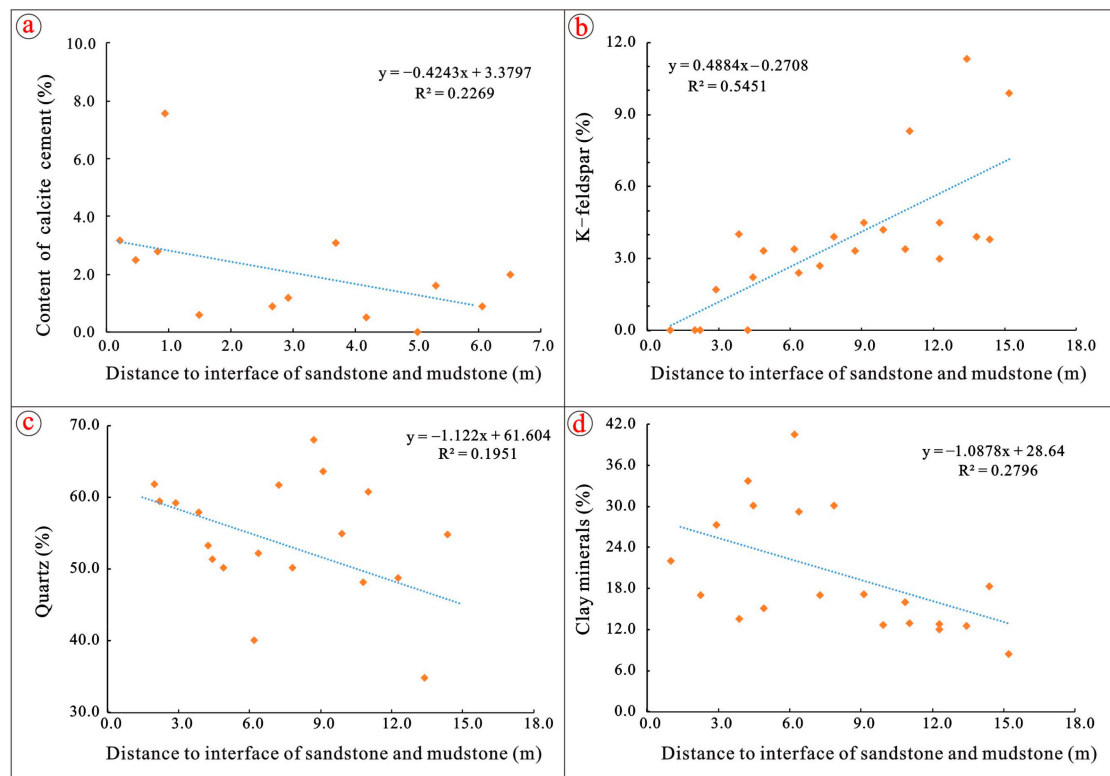
Figure 21. Cross-plot between the distance to interface of sandstone and mudstone and the calcite cements contents (**a**), K- feldspar (**b**), quartz (**c**), and clay minerals (**d**) in the sandstone.

The illite/smectite mixed layer and chlorite/smectite mixed layer in the Lianggaoshan sandstones and shale indicate that illitization of smectite and chloritization of smectite were important transformations of clay minerals during the burial process [47,48] (Supplementary File). The K$^+$, which was necessary for illitization of smectite, was mainly released by potassium feldspar dissolution [49]. The content of potassium feldspar generally decreases with deceasing distance to the interface of sandstone and mudstone (Figure 21b). This can be interpreted as indicating that the potassium feldspar dissolution at the boundary of sandstone was more pervasive than in the center of sandstone (Figure 20). The content of potassium (K) in the shale (e.g., layer3) was higher than that in the sandstone (e.g., layer6 and layer8) (Figure 12). Additionally, the potassium (K) content of sandstone increases with deceasing distance to the interface of sandstone and mudstone (Figure 12). These indicate the K$^+$ released by potassium feldspar dissolution migrated from sandstone into mudstone (Figure 22). The smectite and kaolinite will transform into the chlorite in the absence of K$^+$ [50]. The K$^+$ released by potassium feldspar dissolution migrated from sandstone into mudstone. Therefore, the chlorite coat mainly occurs in the center of sandstone (Figure 10a,b).

Authigenic kaolinite and quartz are the main products of feldspar dissolution [51–54] (Figure 7f). There is a negative correlation between quartz content within sandstone and the distance to the interface of sandstone and mudstone (Figure 21c). The average distance travelled for a silica quantum was 1.15 ± 2.02 m in a direction normal to the stratigraphy [10]. This indicates that some silica exported from the shale was imported by the sandstone boundary [10] (Figure 21c). These indicate that feldspar dissolution produced more authigenic quartz at the sandstone boundary than in the sandstone center, because organic acid mainly migrated from shale into sandstone (Figure 22). There was more detrital quartz and feldspar in the sandstone than in the shale (Supplementary File). Silica transport between shales and sandstones was very limited [10,55] Therefore, the silicon in the sandstone is generally more enriched than in the shale (Figure 12).
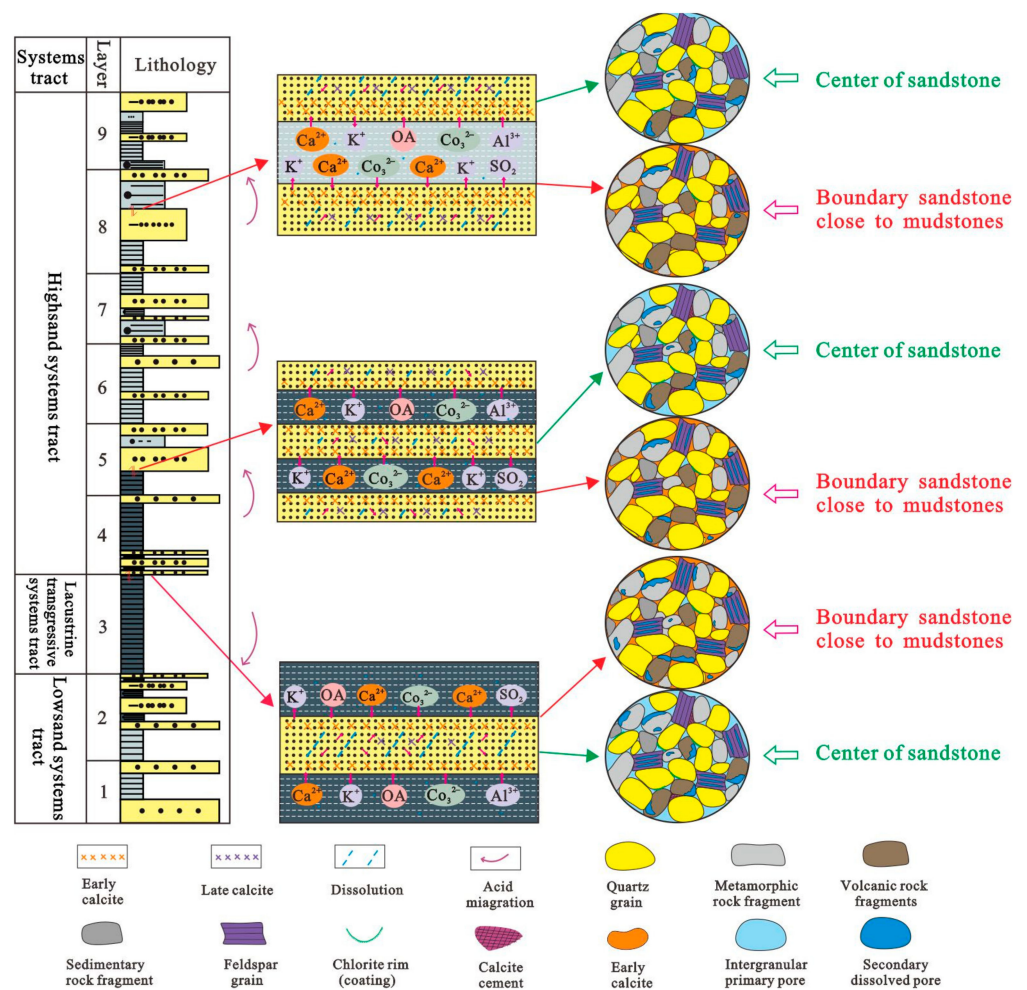
Figure 22. Coevolutionary model of tight sandstone and shale reservoir.

The aluminum (Al) element was more enriched in the shale than in the main sandstone (e.g., layer6 and layer8) (Figure 12). This can be interpreted as indicating that there were significantly more clay minerals in the sandstone than in the shale (Supplementary File), because aluminum mainly occurs in the clay minerals and feldspar. However, the aluminum content of sandstone and shale was almost consistent from layer1 to layer5 (Figure 12). The maximum content of aluminum is in the layer3 (Figure 12). The sand–shale association mainly consists of shale sandwich sandstone and shale sandwich sandstone types in the layer5 and layer9 (Figures 2, 3 and 12). The clay minerals within sandstone increase with deceasing distance to the interface of sandstone and mudstone (Figure 21d). These indicate that aluminum migrated from shale into adjacent sandstone as clay minerals in the shale sandwich sandstone and shale sandwich sandstone (Figure 22).

5.4. Diagenetic Evolution of Tight Sandstone and Shale Reservoir

The compaction of sandstone and shale started in the early eodiagenesis and persisted during the mesodiagenesis burial process (Figure 19). The dark shale generated abundant organic acid (carboxylic acid) and a small amount of hydrocarbon at the early stage of mesodiagenesis (Figures 19 and 20). Therefore, some intergranular dissolution pores and intercrystal pores were formed in the shale due to dissolution at the early stage of mesodiagenesis (Figures 19, 20 and 22). Faults and fractures within the Lianggaoshan Formation were caused by the burial compaction and tectonic compression during Yanshanian and Himalayan cycles [24–26] (Figure 19). The Lianggaoshan Formation dark shale started to produce abundant hydrocarbon in the early Cretaceous period (Figure 20), so that the

intergranular dissolution pores, intercrystal pores and micro-fractures were filled with asphalt (Figure 15).

The chloritization of smectite mainly occurred in an alkaline environment with abundant Al^{3+}, Fe^{2+} and Mg^{2+}, which were generally sourced from alkaline dissolution of basic volcanic rock fragments [56,57] (Figures 4 and 5). Therefore, the chloritization of smectite mainly occurred during eodiagenesis and before massive input of organic acid (Figures 19 and 20). Diagenesis at the sandstone boundary was influenced by organic acid from the shale (Figure 22). Therefore, the chlorite coats mainly occurred in the center of sandstone and precipitated during eodiagenesis (Figure 10a,b). The porosity increases with increasing distance to the interface of sandstone and mudstone (Figure 11b–d). These indicate that chlorite coats were beneficial to protection of primary pore space in the CC sandstone (Figures 7c,e, 16, 17 and 22).

The calcite cement preferentially precipitated at the boundary of sandstone compared with the center of sandstone due to thermal evolution of shale and input of Ca^{2+} and CO_3^{2-} (Figures 21a and 22). The calcite cement mainly precipitated in the late stage of eodiagenesis (Figure 19). The porosity of sandstone decreases with increasing content of calcite cement and deceasing distance to the interface of sandstone and mudstone (Figure 11). These indicate that calcite cement was not conducive to reservoir development due to destruction of primary pores (Figures 21a and 22).

The Lianggaoshan Formation shale generated abundant organic acid (carboxylic acid) and a small amount of hydrocarbon at the early stage of mesodiagenesis (Figure 20). Additionally, secondary dissolution pores were mainly developed at the interface of sandstone and shale (Figures 3, 7g and 11a). Therefore, dissolution mainly occurred at the early stage of mesodiagenesis due to organic acids input from dark shale (Figure 19).

There was only a slight negative correlation between the calcite and the interface of sandstone and shale (Figure 21a). Calcite cement was partially dissolved by organic acids from dark shale (Figure 7a,b), so that the calcite content was heterogeneous in the boundary of sandstone (Figures 7a,b and 21a). Therefore, calcite cement could protect some primary pores from compaction and release pore space by dissolution (Figures 7a,b, 21a and 22).

Some silica exported from the shale was imported by the sandstone boundary. The porosity increases with increasing distance to the interface of sandstone and mudstone (Figure 11b–d). The porosity in the center of sandstone was generally higher than at the interface of sandstone and mudstone (Figure 22). These indicate that the porosity of sandstone and shale was mainly controlled by the thickness of sandstone and dark shale (Figures 21 and 22). The sand–shale association of the Lianggaoshan Formation was determined by system tract and sedimentary environment [22] (Figures 2 and 3). Furthermore, the porosity of sandstone in the highstand system tract was usually higher than that of the sandstone of other layers in the lowstand system tract and lake transgression system tract (Figures 2 and 3). Consequently, the sandstone porosity of sandstone dominant type was usually higher than that in the types of shale dominated and shale-sandstone mixed lithological association (Figure 22). On the contrary, the porosity of shale in the shale dominant type was usually higher than that in the types of sandstone dominated and shale-sandstone mixed lithological association (Figure 22).

6. Conclusions

This study revealed the coevolutionary mechanism of tight sandstone and shale reservoirs within the lacustrine-delta system of the Formation in the Eastern Sichuan Basin, SW China, including the following:

1. The dark shale of the layer3 was the most important source rock within the Lianggaoshan Formation. It reached mature—high mature stage and the shale started to generate abundant organic acid (carboxylic acid) and a small amount of hydrocarbon at the early stage of mesodiagenesis and produce abundant hydrocarbon and some acids in the early Cretaceous period.

2. The pore water with high concentrations of Ca^{2+} and CO_3^{2-} entered the sandstone reservoir from dark shale due to the shale compaction. Potassium feldspar dissolution in the boundary of sandstone was more pervasive than in the center of sandstone. The K^+ released by potassium feldspar dissolution migrated from sandstone into mudstone. Chlorite coat mainly occurs in the center of sandstone. Some silica exported from the shale was imported by the sandstone boundary.

3. The compaction of sandstone and shale started in the early eodiagenesis and persisted during the mesodiagenesis burial process. Some intergranular dissolution pores and intercrystal pores were formed in the shale due to dissolution at the early stage of mesodiagenesis. Chloritization of smectite mainly occurred at eodiagenesis and before massive input of organic acid. Chlorite coats were beneficial to protection of primary pore space in the CC sandstone.

4. Calcite cement preferentially precipitated at the boundary of sandstone compared with the center of sandstone. Calcite cement was not conducive to reservoir development due to destruction of primary pores. Dissolution mainly occurred at the early stage of mesodiagenesis due to organic acids input from the dark shale. Calcite cement also could protect some primary pores from compaction and release pore space by dissolution.

5. These indicate that the porosity of sandstone and shale was mainly controlled by the thickness of sandstone and dark shale. The sandstone porosity of sandstone dominant type was usually higher than that of the types of shale dominant and shale–sandstone mixed lithological association. On the contrary, the porosity of shale in the shale dominant type was usually higher than that of the sandstone dominant types and shale-sandstone mixed lithological association.

Author Contributions: Conceptualization, N.J., X.W. and L.L.; methodology, X.Y., Z.L. and H.Z.; validation, X.T., L.L. and N.J.; formal analysis, J.L., H.Z., Y.Z. and Y.G.; resources, L.L., X.T. and Y.Z.; data curation, H.Z., J.L., X.G. and Y.G.; writing—original draft preparation, H.Z., N.J., X.W. and L.L.; writing—review and editing, N.J., J.G., X.W. and X.T.; visualization, N.J., S.T. and J.W.; supervision, X.T. and L.L.; project administration, X.W. and L.L.; funding acquisition, X.W., X.T. and L.L. All authors have read and agreed to the published version of the manuscript.

Data Availability Statement: The original contributions presented in the study are included in the article and Supplementary Materials, further inquiries can be directed to the corresponding authors.

Conflicts of Interest: Author Yixin Zhuu and Zhouling Li were employed by the PetroChina Southwest Oil & Gas Field Company and Chuangqing Drilling Engineering Company Limited. The remaining authors declare that the research was conducted in the absence of any commercial or financial relationships that could be construed as a potential conflict of interest.

References

1. Jia, C.Z.; Zou, C.N.; Li, J.Z.; Li, D.H.; Zheng, M. Evaluation criteria, major types, characteristics and resource prospects of tight oil in China. *Pet. Res.* **2016**, *1*, 9. [CrossRef]
2. Wu, S.T.; Zhu, R.K.; Yang, Z.; Mao, Z.G.; Cui, J.W.; Zhang, X.X. Distribution and characteristics of lacustrine tight oil reservoirs in China. *J. Asian Earth Sci.* **2018**, *178*, 20–36. [CrossRef]

3. Zhu, R.K.; Zou, C.N.; Mao, Z.G.; Yang, H.B.; Hui, X.; Wu, S.T.; Cui, J.W.; Su, L.; Li, S.; Yang, Z. Characteristics and distribution of continental tight oil in China. *J. Asian Earth Sci.* **2019**, *178*, 37–51. [CrossRef]

4. He, W.Y.; Bai, X.F.; Meng, Q.A.; Li, J.H.; Zhang, D.Z.; Wang, Y.Z. Accumulation geological characteristics and major discoveries of lacustrine shale oil in Sichuan Basin. *Acta Pet. Sin.* **2022**, *43*, 885–898.

5. Wang, F.; Chen, R.; Yu, W.; Tian, J.C.; Liang, X.W.; Tan, X.F.; Gong, L. Characteristics of lacustrine deepwater fine-grained lithofacies and source-reservoir combination of tight oil in the triassic chang 7 member in Ordos Basin, China. *J. Pet. Sci. Eng.* **2021**, *202*, 108429. [CrossRef]

6. Zhu, W.L.; Li, J.P.; Zhou, X.H.; Guo, Y.H. Neogene Shallow Water Deltaic System and Large Hydrocarbon Accumulations in Bohai Bay, China. *Acta Sedimentol. Sin.* **2008**, *26*, 575–582.

7. Huang, D.; Yang, G.; Yang, Z.; Yang, T.Q.; Bai, R.; Li, Y.C.; Dai, H.M. New understanding and development potential of tight oil exploration and development in Sichuan Basin. *Nat. Gas Geosci.* **2019**, *30*, 1212–1221.

8. Jiang, Y.Q.; Qi, L.; Deng, H.B.; Wang, Y.J.; Jiang, C.; Luo, M.S. Hydrocarbon accumulation conditions and exploration potentials of the Jurassic reservoirs in the Sichuan Basin. *Nat. Gas Ind.* **2010**, *30*, 22–26.

9. Yang, Y.M.; Huang, D. Geological characteristics and new understandings of exploration and development of Jurassic lacustrine shale oil and gas in the Sichuan Basin. *Nat. Gas Ind.* **2019**, *39*, 22–33.

10. Gluyas, J.; Garland, C.; Oxtoby, N.H.; Hogg, A.J.C. Quartz cement: The Miller's Tale. *Quartz Cem. Sandstones* **2000**, *29*, 199–218.

11. Burley, S.D. Models of burial diagenesis for deep exploration plays in Jurassic fault traps of the Central and Northern North Sea. *Geol. Soc.* **1993**, *4*, 1353–1375. [CrossRef]

12. Morad, S.; Al-Ramadan, K.; Ketzer, J.M.; De Ros, L.F. The impact of diagenesis on the heterogeneity of sandstone reservoirs: A review of the role of depositional facies and sequence stratigraphy. *AAPG Bull.* **2010**, *94*, 1267–1309. [CrossRef]

13. Liu, M.J.; Liu, Z.; Sun, X.M.; Wang, B. Paleoporosity and critical porosity in the accumulation period and their impacts on hydrocarbon accumulation—A case study of the middle Es3 member of the Paleogene formation in the Niuzhuang Sag, Dongying Depression, Southeastern Bohai Bay Basin, East China. *Pet. Sci.* **2014**, *11*, 495–507.

14. Yang, T. Synergistic Diagenetic Evolution of Deep-Water Gravity FlowSandstones-Mudstones and Genesis of High Quality Reservoirs in the Third Member of the Shahejie Formation, Dongying Depression. Ph.D. Thesis, China University of Petroleum, Beijing, China, 2017.

15. Meng, Q.A.; Zhang, S.; Sun, G.X.; Fu, X.L.; Wang, C.; Shang, Y. A seismic geomorphology study of the fluvial and lacustrine-delta facies of the Cretaceous Quantou-Nenjiang Formations in Songliao Basin, China. *Mar. Pet. Geol.* **2016**, *78*, 836–847.

16. Jia, J.L.; Bechtel, A.; Liu, Z.J.; Strobl, S.A.I.; Sun, P.C.; Sachsenhofer, R.F. Oil shale formation in the Upper Cretaceous Nenjiang Formation of the Songliao Basin (NE China): Implications from organic and inorganic geochemical analyses. *Int. J. Coal Geol.* **2013**, *113*, 11–26. [CrossRef]

17. Wang, C.; Wang, Q.X.; Chen, G.J.; He, L.; Xu, Y.; Chen, L.Y.; Chen, D.F. Petrographic and geochemical characteristics of the lacustrine black shales from the Upper Triassic Yanchang Formation of the Ordos Basin, China: Implications for the organic matter accumulation. *Mar. Pet. Geol.* **2017**, *86*, 52–65. [CrossRef]

18. Zou, J.; Jin, T.; Li, X.S.; Wei, T.Q.; Guo, R.Y.; Bai, R. Evaluation on exploration potentials of Lower Jurassic reservoirs in eastern Sichuan Basin. *China Pet. Explor.* **2018**, *23*, 30–38.

19. Shi, L.Z.; Wang, Z.Z.; Zhang, G.; Zhang, Y.S.; Xing, E.Y. Distribution and formation of tight oil in Qijia area, Songliao Basin, NE China. *Pet. Explor. Dev.* **2015**, *42*, 44–50. [CrossRef]

20. Chen, S.J.; Zhang, H.X.; Lu, J.G.; Yang, Y.M.; Liu, C.W.; Wang, L.; Zou, X.L.; Yang, J.J.; Tang, H.P.; Yao, Y.T.; et al. Controlling factors of Jurassic Da'anzhai Member tight oil accumulation and high production in central Sichuan Basin, SW China. *Pet. Explor. Dev.* **2015**, *42*, 206–214. [CrossRef]

21. Yang, X.P.; Zou, C.N.; Tao, S.Z.; Wang, Z.C.; Li, J.; Wang, S.Q. Characteristics of upper Triassic-Jurassic oil and gas system in Sichuan basin and oil and gas abundance law. *China Pet. Explor.* **2005**, *10*, 15–22.

22. Yu, X.; Yang, Y.X.; Zhou, H.H.; Luo, B.; Luo, L.; Luo, X.; Zhu, Y.X.; Chen, W.D.; Chen, S.C.; Liu, F.; et al. Genetic mechanism of tight sandstone reservoir of lacustrine-delta sand-mud interlayer in Lianggaoshan Formation of Jurassic. eastern Sichuan Basin. *Nat. Gas Geosci.* **2023**, *34*, 1595–1611.

23. Zou, Y.T.; Duan, J.B.; Zhao, Y.J.; Zhang, X.; Li, R.B. Tectonic characteristics and evolution of the high and steep fault folding belt in east Sichuan. *Acta Geol. Sin.* **2015**, *89*, 2046–2052.

24. Liu, S.F.; Steel, R.; Zhang, G.W. Mesozoic sedimentary basin development and tectonic implication, northern Yangtze Block, eastern China: Record of continent–continent collision. *J. Asian Earth Sci.* **2005**, *25*, 9–27. [CrossRef]

25. Li, Z.Q.; Ran, L.H.; Chen, G.S.; Lu, Z.K.; Duan, X.G. Genetic geologic model and gas-bearing analysis of high steep structures in east Sichuan. *J. Chengdu Univ. Technol. Sci. Technol. Ed.* **2002**, *29*, 605–609.

26. Zhang, X.H. *Study on Structural Characteristics and Genetic Mechanism of Barrier Folds in Eastern Sichuan*; Chengdu University of Technology: Chengdu, China, 2019.

27. Li, J.; Tao, S.Z.; Wang, Z.C.; Zou, C.N.; Gao, X.H.; Wang, S.Q. Characteristics of Jurassic Petroleum Geology and Main Factors of Hydrocarbon Accumulation in NE Sichuan Basin. *Nat. Gas Geosci.* **2010**, *21*, 732–741.

28. Wu, Y.Y.; Zhang, T.S.; Tao, S.Z.; Feng, R.C. Sequence Stratigraphy of Depositional Sandbodies in the Deep-water Lake Basin: A case from Jurassic Sichuan. *Acta Sedimentol. Sin.* **2013**, *31*, 798–806.

29. Zhang, T.S.; Tao, S.Z.; Wu, Y.Y.; Yang, J.J.; Pang, Z.L.; Yang, X.P.; Chen, Y.Y.; Yuan, M.; Liu, M.; Fan, J.W. Control of sequence stratigrapnic evolution on the types and distribution of favorable reservoir in the delta and beach-bar sedimentary system: Case study of Jurassic Lianggaoshan Formation in Centra Sichuan Basin, China. *Acta Sedimentol. Sin.* **2019**, *30*, 1286–1300.

30. Yi, J.Z.; Zhang, S.M.; Cai, L.X.; Chen, S.C.; Luo, X.; Yu, J.X.; Luo, N.N.; Yang, T. Strata and Sedimentary Filling Characteristics of the Lower Jurassic Lianggaoshan Formation and Its Hydrocarbon Exploration in Eastern Sichuan Basin. *J. Jilin Univ. Earth Sci. Ed.* **2022**, *52*, 795–815.

31. Li, C.X.; He, D.F.; Sun, Y.P.; He, J.Y.; Jiang, Z.X. Structural characteristic, and origin of intra-continental fold belt in the eastern Sichuan Basin, South China Block. *J. Asian Earth Sci.* **2015**, *111*, 206–221. [CrossRef]

32. Yuan, G.H.; Gluyas, J.; Cao, Y.C.; Oxtoby, N.H.; Jia, Z.Z.; Wang, Y.Z.; Xi, K.L.; Li, X.Y. Diagenesis and reservoir quality evolution of the Eocenes and stones in the northern Dongying Sag, BohaiBay Basin, East China. *Mar. Pet. Geol.* **2015**, *62*, 77–89. [CrossRef]

33. Luo, L.; Gao, X.Z.; Gluyas, J.; Tan, X.F.; Cheng, C.L.; Kong, X.Y.; Qu, F.T.; Shao, H.B. Reservoir quality prediction of deeply buried tight sandstones in extensively faulted region: A case from the Middle-Upper Jurassic Shishugou Group in central Junggar Basin, NW China. *J. Pet. Sci. Eng.* **2019**, *175*, 22–45. [CrossRef]

34. Folk, R.L. *Petrology of Sedimentary Rocks*; Hemphill Publishing Co.: Austin, TX, USA, 1980.

35. Li, N.; Hong, H.T.; Li, G.H.; Zhou, H.F.; Jia, M.; Kang, J.H. Geological characteristics of shale oil and gas of Lianggaoshan Formation in high-steep structural zone, Sichuan Basin. *Nat. Gas Explor. Dev.* **2022**, *45*, 86–95.

36. Qing, Y.H.; Lv, J.Y.; Wu, J.Y.; Yang, Y.Y.; Zhang, S.L.; Xiong, S.H.; Liu, J.F. Formation mechanisms of calcite cements in tight sandstones of the Jurassic Lianggaoshan Formation, northeastern Central Sichuan Basin. *Aust. J. Earth Sci.* **2019**, *66*, 723–740. [CrossRef]

37. Surdam, R.C.; Crossey, L.J.; Hagen, E.S.; Heasler, H.P. Organic-inorganic interactions and sandstone diagenesis. *AAPG Bull.* **1989**, *73*, 1–23.

38. Barth, T.; Bjørlykke, K. Organic acids from source rock maturation: Generation potentials, transport mechanisms and relevance for mineral diagenesis. *Appl. Geochem.* **1993**, *8*, 325–337. [CrossRef]

39. Xu, H.M.; Lin, Y.X.; Xi, F.Y.; Fang, L.F. The organic acid evolution and distribution of Eogene in Mangya depression. *Pet. Explor. Dev.* **2000**, *27*, 23–25.

40. Tissot, B.P.; Welte, D.H. *Petroleum Formation and Occurrence: A New Approach to Oil and Gas Exploration*; Springer: Berlin/Heidelberg, Germany, 1978; 538p.

41. Zuo, Y.H.; Wang, C.C.; Tang, S.L.; Hao, Q.Q. Mesozoic and Cenozoic thermal history and source rock thermal evolution of the Baiyinchagan sag, Erlian Basin, Northern China. *J. Pet. Sci. Eng.* **2016**, *139*, 171–184. [CrossRef]

42. Wang, X.X.; Zhou, S.X. Influence of mudstone diagenesis on cementation of sandstone reservoir. *Acta Pet. Sin.* **1992**, *13*.

43. Tan, X.F.; Ran, T.; Luo, L.; Wang, J.; Liang, M.; Chen, Q.; Kuang, H. The "sand-mud" sedimentary record and its Diagenetic system in shore-shallow Lacustrine—A case study of Eocene Kongdian Formation in Jiyang Depression. *Adv. Earth Sci.* **2016**, *31*, 615–633.

44. Dutton, S.P. Calcite cement in Permian deep-water sandstones, Delaware Basin, west Texas: Origin, distribution, and effect on reservoir properties. *AAPG Bull.* **2008**, *9*, 765–787. [CrossRef]

45. Carvalho, M.V.F.; De Ros, L.F.; Gomes, N.S. Carbonate cementation pattern and diagenetic reservoir facies in the Campos Basin cretaceous turbidites, offshore eastern Brazil. *Mar. Pet. Geol.* **1995**, *12*, 741–758. [CrossRef]

46. Li, Q.; Jiang, Z.X.; Liu, K.Y.; Zhang, C.M.; You, X.L. Factors controlling reservoir properties and hydrocarbon accumulation of lacustrine deep-water turbidites in the Huimin depression, Bohai Bay Basin, East China. *Mar. Pet. Geol.* **2014**, *57*, 327–344. [CrossRef]

47. Meunier, A. *Clays*; Springer: Berlin/Heidelberg, Germany, 2005.

48. Day-Stirrat, R.J.; Milliken, K.L.; Dutton, S.P.; Loucks, R.G.; Hillier, S.; Aplin, A.C.; Schleicher, A.M. Open-system chemical behavior in deep Wilcox Group mudstones, Texas Gulf Coast, USA. *Mar. Pet. Geol.* **2010**, *27*, 1804–1818. [CrossRef]

49. Hower, J.; Eslinger, E.V.; Hower, M.E.; Perry, E.A. Mechanism of burial metamorphism of argillaceous sediment: 1. Mineralogical and chemical evidence. *GSA Bull.* **1976**, *87*, 725–737. [CrossRef]

50. Ying, F.X.; Luo, P.; He, D.B. *The Diagenesis and Diagenetic Modeling of Clastic Reservoirs in the Petroliferous Basins in China*; Pet Industry Press: Beijing, China, 2004; pp. 56–59.

51. Huang, S.J.; Xie, L.W.; Zhang, M.; Wu, W.H.; Sheng, L.C.; Liu, J. Formation mechanism of authigenic chlorite and relation to preservation of porosity in nonmarine Triassic reservoir sandstones, Ordos Basin and Sichuan Basin, China. *J. Chengdu Univ. Technol. Sci. Technol. Ed.* **2004**, *31*, 273–281.

52. Peltonen, C.; Marcussen, Ø.; Bjørlykke, K.; Jahren, J. Clay mineral diagenesis and quartz cementation in mudstones: The effects of smectite to illite reaction on rock properties. *Mar. Pet. Geol.* **2009**, *26*, 887–898. [CrossRef]

53. Thyberg, B.; Jahren, J.; Winje, T.; Bjørlykke, K.; Faleide, J.I.; Marcussen, Ø. Quartz cementation in Late Cretaceous mudstones, northern North Sea: Changes in rock properties due to dissolution of smectite and precipitation of microquartz crystals. *Mar. Pet. Geol.* **2010**, *27*, 1752–1764. [CrossRef]

54. Wilkinson, M.; Haszeldine, R.S. Oil charge preserves exceptional porosity in deeply buried, overpressured, sandstones: Central North Sea, UK. *J. Geol. Soci.* **2011**, *168*, 1285–1295. [CrossRef]

55. Bjørlykke, K.; Jahren, J. Open or closed geochemical systems during diagenesis insedimentary basins: Constraints on mass transfer during diagenesis and the prediction of porosity in sandstone and carbonate reservoirs. *AAPG Bull.* **2012**, *96*, 2193–2214. [CrossRef]

56. Yuan, Z.; Zheng, Y.Z.; Yuan, H.L.; Yang, X.Y.; Li, W.H. Study on the characteristics and diagenesis model of laumontite cement in Yanchang Formation in the southeastern margin of Ordos Basin. *J. Northwest Univ. Nat. Sci. Ed.* **2020**, *50*, 124–134, (In Chinese with English Abstract).
57. Tan, D.P.; Luo, L.; Song, L.; Liu, F.; Wang, J.X.; Gluyas, J.; Zhou, H.H.; Wang, J.; Zhu, C.B.; Mo, S.Y.; et al. Differential precipitation mechanism of cement and its impact on reservoir quality in tight sandstone: A case study from the Jurassic Shaximiao formation in the central Sichuan Basin, SW China. *Geoenergy Sci. Eng.* **2023**, *221*, 111263. [CrossRef]